A study of the effects of weathering on soils derived from decomposed volcanic rocks

OKEWALE, Ismail Adeniyi[1] and COOP, Matthew Richard[2]

Author Affiliations

[1]PhD student, City University of Hong Kong

Tat Chee Avenue, Kowloon, Hong Kong.

iaokewale2-c@my.cityu.edu.hk (Corresponding Author)

[2]Professor of Geotechnical Engineering

University College London, formerly City University of Hong Kong.

m.coop@ucl.ac.uk

ABSTRACT

A comprehensive investigation was made of the effects of weathering on the nature and mechanics of volcanic saprolites from Hong Kong. Few such studies have been conducted in volcanic weathered soils and the application of a critical state type of framework that accounts for the effects of structure, as has been used here, is especially novel. The investigation examined the effects of spatial variations of the effects of weathering both vertically as the weathering degree alters, and horizontally through comparing data from different sites. In addition to index tests, SEM and XRD, an extensive series of oedometer, triaxial and multi-directional bender elements tests was carried out, comparing the behaviour of samples from different locations and depths in both intact and reconstituted states. This meant that the changes to the intrinsic (reconstituted) behaviour could be traced throughout different degrees of weathering along with the effects of changing structure on the mechanical behaviour of the intact soils. The intrinsic properties changed in a manner that was broadly consistent with the increasing of fines content and plasticity due to weathering. The effects of meso-structure were small to medium in compression, and in shearing they were generally even less evident, both at small strains and failure. The degrees of anisotropy of stiffness for both intact and reconstituted samples were mostly quite small.

KEYWORDS: weathering; geological structure; critical state framework; anisotropy

1. INTRODUCTION

In weathered sedimentary soils in temperate regions there have been extensive and detailed studies of the effects of weathering on mechanical behaviour, for example Chandler (1972) or Cafaro and Cotechia (2001), who investigated the effects of weathering on the structure of a

sedimentary clay and its link to the mechanical behaviour within a critical state framework. Similarly, there are many studies of the effects of weathering in saprolites created from rocks of igneous origin in tropical and sub-tropical regions (e.g. Alavi Nezhad Khalil Abad et al., 2014; Alavi Nezhad Khalil Abad et al., 2016; Basu, 2009; Basu et al., 2009; Futai et al., 2004; Irfan, 1996, 1999; Ng and Chiu, 2001; Wang and Yan, 2006). However, there have been very few attempts to examine the behaviour of weathered saprolites within a critical state based approach that includes the effects of structure like those that Burland (1990) and Cotecchia and Chandler (2000) have developed for sedimentary soils. There is no reason why frameworks developed for sedimentary soils should a priori be applicable, since in a sedimentary soil the structure (fabric and bonding) is formed by depositional and post-depositional processes, tending generally to add strength and stiffness to the intrinsic soil behaviour, while in saprolitic soils the mode of creation is the reverse, being one of disintegration of parent rocks, a process that weakens and softens it. The mode of their formation also affects not only the structure but the underlying intrinsic behaviour as the constituent particles of the soil are modified by the weathering processes. Volcanic rocks may also have a higher initial variability in the distribution of particle sizes, shapes and mineralogy. Rocchi and Coop (2015) successfully applied these techniques to granitic saprolites but otherwise there are very few similar attempts and the investigation of the general applicability of frameworks developed for sedimentary soils to soils derived from weathered rocks is therefore one key motivation behind this work.

Some studies have provided significant insight into the mechanical behaviour of some of these geomaterials, and for example Futai et al. (2004) studied a gneissic saprolitic soil along a 7m profile, finding that the in-situ specific volume reduced with depth. Wang and Yan (2006) studied two common saprolites from Hong Kong but only from one location and quite narrow depth ranges. Their study revealed that intact samples exhibited a yield stress that was not abrupt but rather gradual in isotropic loading which they concluded was the result of the

presence of bonding. Rocchi and Coop (2015) studied extensively the effects of weathering on the physical and mechanical behaviour of granitic saprolites also from Hong Kong along a profile up to a depth of 40m, but again only from one location. They found that as the weathering increased (or depth reduced) there were clear changes to the mineralogy that accompanied a grading that became finer and better graded, while the in-situ specific volume increased and the effects of structure reduced.

The alteration in volcanic rocks in Hong Kong is caused by chemical and physical processes similar to those affecting granitic rocks (Irfan, 1996a; 1999). Due to the subtropical climatic conditions of Hong Kong, hydrolysis, solution and oxidation are the important chemical processes that usually cause the alteration. Hydrolysis and solution cause the removal of cations from the feldspars, and in free drained areas such as hillsides and slopes, commonly found in Hong Kong, kaolinites and the halloysites are the clay minerals that are formed while in areas that are stagnant, expansive clays such as montmorillonites and illites are formed. In iron bearing rocks (e.g. biotite), oxidation and reduction play an important role by converting iron to haematite and goethite. The physical processes that cause the alteration in volcanic rocks are repeated wetting and drying that can cause disintegration. The degree of alteration depends on variations of the mineralogy and texture of the rocks, local variations in joint spacing, topography, prevalence of erosion, vegetation, ground water and climatic conditions.

In this paper, the evolution of the physical properties and mechanical behaviour of saprolites from volcanic rocks (locally called tuff) are investigated covering a wide range of weathering degrees ranging from Highly Decomposed Volcanic rocks (HDV) to Completely Decomposed Volcanic rocks (CDV). These are the most common geomaterials in Hong Kong, but have received less attention than the Completely Decomposed Granite (CDG), which is more usually encountered in urban areas, but the HDV/CDV is of increasing importance as urbanisation spreads into the New Territories and the south of Hong Kong Island. The samples

had been retrieved from a variety of locations, from a range of depths and from different formations, allowing some assessment to be made of the overall variability of the effects of weathering and engineering behaviour. The physical properties were investigated through classification and index tests, the microstructure examined for both intact and reconstituted samples through SEM and the mineralogy through XRD. The mechanical behaviour was investigated by carrying out extensive oedometer and triaxial tests on both intact and reconstituted samples. The data obtained from these tests are interpreted and discussed using a critical state framework that accounts for the effects of structure, complementing a similar study by Rocchi and Coop (2015) on the CDG, this being the first such comprehensive investigation using a structure based critical state framework of the mechanical effects of weathering in a volcanic saprolite. The application of a critical state framework that accounts for the effects of structure to these soils will be of general interest to other saprolitic soils which are abundant in tropical and subtropical regions.

2. MATERIALS, APPARATUS AND EXPERIMENTAL PROCEDURES

The soils tested were saprolites from volcanic rocks. The majority of the samples belonged to Ap Lei Chau formation, while a few samples were taken from the Mount Davis formation. The Early Cretaceous Ap Lei Chau formation is composed predominantly of fine ash vitric tuffs, while the Mount Davis formation is of similar age but is formed predominantly of coarse ash crystal tuff. Both formations have some degree of heterogeneity, however, which is typical of extrusive and pyroclastic rocks.

The samples were taken as blocks and Mazier rotary cores from Hong Kong Island (Figure 1) under the supervision of the Hong Kong Geotechnical Engineering Office. The block samples were recovered from trial pits and are therefore shallower in depth, ranging from 0.7m to 2.6m,

while the Mazier samples ranged from 1m to 14m. The shallower weathering that is typical of the volcanic saprolites compared to the granitic, meant that deeper samples, as tested for the CDG by Rocchi and Coop (2015), were not available. The characteristics of the samples are shown in Table1. The visual descriptions of the samples given in the table were made at the time of sampling by the engineers or geologists on site, and are based on the GEO (1988) six grade classification, these samples corresponding to grades IV and V, Highly and Completely Decomposed, respectively (Irfan, 1996; ISRM, 2007). Refinements were added to the descriptors, and these are extremely weak (ew), extremely weak to very weak (ewvw), very weak (vw), very weak to weak (vww), weak (w), and weak to moderately weak (wmw). All descriptions are to some extent subjective, but each one was verified by the authors in the laboratory on opening the samples using visual inspection and the slaking method. Both the block and Mazier samples had a variety of colours, which might be as a result of the variability of the parent rocks and/or the presence of sesquioxides. While the weathering penetration tends not to be as deep in the volcanics as in the granites in Hong Kong, both are strongly affected by the joint structure. The weathering degree of the samples therefore shows a relatively poor correlation with depth. Because the samples are from different locations, the degree of weathering at a given depth would also be affected by factors such as, local variation in joint spacing, topography, prevalence of erosion and vegetation.

A combination of wet sieving and sedimentation was used to determine the gradings. The microstructure of the intact and reconstituted samples was investigated using a Philips XL30 FEG Environmental Scanning Electron Microscope (ESEM) equipped with an energy dispersive X-ray spectrometer (EDXS). The tested samples were taken by breaking surfaces, rather than cutting, to give a true reflection of the fabric. The bulk mineralogy of the soils was studied using Bruker X-ray diffractometer, analysing samples in powder form.

123 Conventional front-loading oedometers were used to investigate the one-dimensional
124 compression behaviour. For tests up to 7MPa the usual fixed confining ring was used, with
125 50mm diameter and 20mm height. To increase the capacity to 20MPa, a smaller 30mm dimeter
126 was used, but this was of a floating ring type, thereby reducing the wall friction. The
127 reconstituted samples were prepared by adding varying amounts of distilled water to create
128 target sample densities. The samples were then poured/placed into the oedometer rings and the
129 initial height carefully taken under a nominal load of about 3kPa. The samples were then
130 flooded, allowing 12-24hrs for saturation before loading in increments to 7MPa.

131 The intact oedometer samples were prepared by trimming the block and Mazier samples
132 very carefully, minimising disturbance, excavating the soil slightly ahead of the ring that was
133 advanced with a small downward pressure. The intact samples were poorly saturated in situ
134 and so saturation was made by inundation of the oedometer under a vertical stress of around
135 10-20kPa, which was found to prevent significant swelling or collapse, either of which might
136 cause destructuration.

137 Conventional triaxial apparatus as well as Imperial College (IC) and GDS stress path
138 triaxial apparatus were used for the investigation of the shearing behaviour, applying cell
139 pressures up to 750kPa for the conventional and IC apparatus and 2MPa for the GDS. Details
140 are given in Table 2. Back pressure saturation was used, which required extended saturation
141 times due to the presence of significant fines, but B values (the ratio of the change in pore
142 pressure to change in cell pressure ($\Delta u/\Delta\sigma_3$)), which is an indication of the completeness of
143 saturation, of over 0.95 were achieved. Both the IC and GDS apparatus were equipped with
144 local instrumentation for the measurement of axial and radial strains as well as bender elements
145 mounted in the platens for the measurement of the elastic shear modulus in the vertical plane,
146 G_{vh}. The samples were of 38mm, 50mm or 75mm diameter each for the conventional, IC and
147 GDS apparatus, all with a 2:1 height to diameter ratio.

148 The reconstituted samples for the triaxial tests were prepared by adding distilled water to the
149 soil to make slurries. Within a critical state framework that accounts for structure (e.g. Burland,
150 1990) the effects of structure (fabric and bonding) are assessed by comparing the behaviour of
151 the intact soil with the same soil in its reconstituted state, the latter giving its "intrinsic" or
152 underlying behaviour resulting solely from the particles that constitute the soil. A complication
153 for a saprolitic soil as compared to typical sedimentary soils, is that weathering may give large
154 changes both to the effect of the structure and also to the intrinsic behaviour. The reconstituted
155 samples therefore made it possible to trace the intrinsic behaviour across all the degrees of
156 weathering together with the changes in the effects of structure of the intact samples.

157 For the 38mm diameter samples, consolidometer that has the same diameter as sample
158 was used for sample preparation. The samples were then extruded, cut to the required height
159 and placed on the platen. For the 50mm diameter samples, it was found to be difficult to extrude
160 and the samples were therefore prepared directly on the platen by pouring the slurry inside a
161 specially designed mould with the same dimension as the samples required.

162 The intact samples for the triaxial tests were again trimmed very carefully by hand on
163 a lathe, which was highly time consuming with frequent failures of samples. The Mazier
164 sample tubes were 75mm in diameter, which were cut to the required length while still in the
165 tube using a diamond tipped rotary saw. Several slots were then carefully cut along the length
166 of the tube using a machine end cutter, while providing support to the sample. The segments
167 of tube between the slots were then carefully peeled off the sample and the perimeter of the
168 samples dressed, any small spaces being filled with remoulded trimmings. This process
169 avoided the disturbance that would occur if the samples were extruded.

170 The specific volumes, v (=1+e), of the samples were very carefully measured, using
171 several methods to make the measurement to improve confidence. Typically, for the intact
172 samples the initial v could be derived from the initial dimensions, weight and water content,

while the final v could be derived from the final water content, back-calculating an initial value using the measured volumetric strain. For the reconstituted samples the initial water content could also be used. A mean of the various initial values was taken and an estimate of the accuracy of the measurement made by taking the largest difference between any individual value and the mean. The estimated accuracies for the triaxial tests are given in Table 2. They are generally within about ±0.03, but a few are greater, indicating the difficulty of obtaining accurate values of v in these heterogeneous soils.

3. SOIL CHARACTERISATION

Figure 2 shows the grading curves for different weathering degrees. Solid lines are used for the HDV and broken lines for the CDV, and the reduction in line weights and lighter colours correspond to the increase in the degree of weathering, a similar scheme being used in all figures so that trends with weathering may be identified more easily. It can be seen that all the soils are well graded and they can all be classified as silty sand. There is some scatter of the data, some of which may be the result of variability in the parent rock grain size. For the extremely weak CDV (ewCDV), the curves are reasonably similar particularly in the fine fraction and apart from the grading curve of the weak-moderately weak HDV (wmwHDV), the most weathered and shallower soils tend to plot above the less weathered soils, with finer gradings, similarly to the CDG (e.g. Rocchi and Coop, 2015).

The gradings are plotted against depth in Figure 3. Filled and open symbols are used for the HDV and CDV respectively and the symbol weights again reduce as the degree of weathering increases. In Figure 3(a), the soils are divided into fines, sand and gravel components, two data points for each sample representing the boundaries of these sizes. The variation of the median size (D_{50}) is shown in Figure 3(b) and apart from the scatter for the

197 samples at shallow depths, it can be seen that the median size seems to increase slightly with
198 depth, at least for the CDV. The coefficient of uniformity (c_u) (Figure 3(c)) confirms that all
199 the samples are very well graded, while the variation of fines with depth in Figure 3(d)
200 generally indicates a small reduction of fines with increased depth and reduced weathering,
201 again at least for the CDV, although the shallow samples of the HDV seem to add to the scatter
202 because they are less weathered. Given that the samples are from numerous different locations
203 and from two formations, the scatter of the index data is not excessive and general trends may
204 be identified.

205 The index properties in terms of plasticity and activity are shown in Figure 4. From the
206 plasticity chart (Figure 4(a)) the soils can be classified as silt, but having a wide range of
207 plasticities. It is interesting to see that the plasticities of the HDV are not so different to the
208 CDV because it might have been expected that weathering would have increased plasticity.
209 However, in Figure 4(b) it can be seen that both *LL* and *PL* increase with *CF*, which tends to
210 confirm an increasing plasticity with weathering. The activities are low and there is no
211 particular trend with weathering, as can be seen in Figure 4(c). The variations of *LL* and *PL*
212 with depth are shown in Figure 3(e) and apart from scattered data at shallower depths the
213 plasticities reduce with increasing depth and reduced weathering, as expected, although the
214 HDV samples again seem anomalous in that they give lower plasticities at shallow depths. The
215 difference observed for the HDV might be as a result of heterogeneity so that a less weathered
216 material is found at these shallow depths. Other factors may be the few data compared to the
217 CDV as well as samples being from different locations. Figure 3(g) shows the profile of the
218 in-situ specific volume measured from the oedometer and triaxial samples. This tends to reduce
219 with depth, part of which must result from increased stress levels but most of which should be
220 associated with changes due to weathering.

221

4. MICROSTRUCTURE AND MINERALOGY

Microscopic observations of the fabric of reconstituted samples from the ESEM micrographs are shown in Figure 5. The micrographs shown are for a 50μm field of view for selected weathering degrees. The reconstitution process produces fairly similar fabrics for all the weathering degrees and the soils appear relatively isotropic as the views in the horizontal and vertical planes are similar. The wCDV appears finer grained, but this is probably just a function of the field of view chosen as overall the grading is coarser (Figure 2). In the larger scale the fabrics seem relatively homogeneous, but locally some heterogeneity is created by flatter particles agglomerating together forming continuous clusters giving some slight local orientation of fabric.

Micrographs of the fabrics of intact samples are shown in Figure 6. The ewCDV (Figure 6(a)) is again characterised by well-arranged flat particles agglomerated to form continuous clusters, with larger inter-cluster voids. The vwwHDV (Figure 6(b)) is more homogeneous and is characterised by well-connected flat particles but without clusters. Samples ewCDV and wCDV have been studied in the horizontal and vertical planes (Figure 6 (c-f)) showing that the natural fabrics of the intact soils are not significantly anisotropic. An orientated fabric in a weathered soil would be most likely to have been inherited from the parent material, as weathering would be unlikely to create new anisotropy. The lack of a preferred orientation might therefore be expected in a weathered igneous rock, in contrast to materials of sedimentary origin for which particle orientation is common. Again there is some local heterogeneity with flat particles clustered together. Closer inspection of the micrographs at a higher magnification suggested that there may be some bonding between particles but that this was not extensive.

The details of elemental composition obtained using EDXS from microstructure analysis are shown in Table 3. The degree of alteration is higher in most weathered soils with low amounts in terms of weight and atomic percentage of feldspar cations. These cation alterations cause the change of some feldspars to clay minerals which are abundant in most weathered soils.

Figure 7 presents the mineralogy of selected samples as obtained from X-ray diffraction. The details of mineralogy for different weathering degrees are shown in Table 4. The mineralogy varies with weathering degree and is labelled on the graphs. The parent rocks of the soils were composed basically of quartz, feldspars, biotites and other accessory minerals. Weathering causes the breaking down of these minerals to clay minerals, quartz being the most resistant to weathering, followed by the feldspars. In the most weathered soils, the mineralogy therefore has a much higher proportion of clay minerals; kaolinites, halloysites, illites and montmorillonites. The most weathered soil has the highest percentage of clay minerals and least percentage of quartz at shallow depths and in contrast, the least weathered soil has the least percentage of clay minerals and percentage of quartz is higher. The profile of mineralogy as presented in Figure 3(f) showing that the clay minerals reduce with depth, feldspars increase with depth and quartz, apart from a lower percentage at very shallow depths, remains relatively unchanged.

5. COMPRESSION BEHAVIOUR

The compression paths for the reconstituted and intact samples in one-dimensional compression are shown in Figure 8 together with the intrinsic normal compression lines (1D-NCL*) interpreted from the reconstituted samples. Reconstituted samples are in broken lines while solid lines are used for the intact with grey or black representing the location and/or

degree of weathering. The 1D-NCL*s chosen are assumed to be straight lines within the range of pressures tested.

For each weathering degree several reconstituted samples were tested with different initial specific volumes, v (=1+e), but in each case the soils did not have a transitional mode of behaviour, with non-convergence of the compression paths, as can be sometimes found for soils that are well graded and/or have complex mineralogies (Altuhafi and Coop, 2011; Ferreira and Bica, 2006; Martins et al., 2001; Shipton and Coop, 2012). Irrespective of the initial state, all the curves converge to unique 1D-NCL*.

Plotting the slopes ($\lambda = C_c/2.303$) and intercepts N_o of the 1D-NCL* with depth, as shown in Figures 9 (b & c), it can be seen that they both reduce significantly with depth. On Figures 10 (a & b) it can be seen that this trend is due to both parameters increasing with fines content (Figures 10, a & b). Within the scatter of the data there is little difference between the two formations and in general the scatter of data is not large considering that the samples are from numerous locations. Comparing the slope λ with similar soils, Futai et al. (2004) found relatively similar values for gneissic residual soils and also Rocchi and Coop (2015) found similar values for granitic saprolite that also tend to reduce with depth. Figure 11 summarises the 1D-NCL*s and it can be seen that the most weathered soils therefore generally tend to plot above the least weathered soils.

The variation of intercept N_o (at σ'_v=1kPa) and compressibility index C_c with mineralogy (clay and quartz) are presented in Figure 12. Figure 12 (c & d) show the relationship between N_0 and clay minerals and quartz content respectively. These do not really show good correlations even if the most weathered soils have high clay mineral and low quartz contents. Also, the relationships between compressibility index ($C_c = \lambda * 2.303$) and mineralogies in

Figures 12 (e) and (f) are quite poor, indicating that mineralogy alone is a poor predictor for mechanical behaviour and probably not as good as fines content.

The compression curves of the intact samples are also shown in Figure 8. The initial in-situ specific volume tends to increase with weathering, as was seen in Figure 3(g). All the samples, except one reach states outside their respective intrinsic normal compression line. The yield stresses will be influenced not only by the effects of structure, but also by the location of the intrinsic normal compression line and the in-situ specific volume. The latter two factors tend to counteract each other, so as the less weathered deeper samples tend to have lower in-situ v but also lower λ and N_o values, so that the change of yield stress with weathering degree is unclear.

For the intact samples in both the oedometer and triaxial tests, sample disturbance was estimated using the criterion $\Delta e/e_0$ suggested by Lunne et al. (1997), where e_0 is the in-situ void ratio and Δe the change measured in the test when restoring the estimated in-situ stress level. From Figure 9(a), the samples can be seen to range from excellent to good.

The initial states of the samples may be quantified by the ratio of in-situ vertical stress $(\sigma'_{v,\,insitu})$ to an equivalent stress on the 1D-NCL*, $\sigma'_{ve}\{= exp((N_0-v)/\lambda))\}$, and the values derived are shown in Figure 13(a). The maximum value possible is 1.0, since the current yield stress cannot be less than the stress experienced in the ground, but in many cases the values are significantly less, indicating that the soil has previously experienced a larger stress, and/or that there is a significant effect of structure.

Figure 14 presents the normalised compression behaviour of the soils in the void index, I_v, plane as proposed by Burland (1990), where $I_v=(e-e^*_{100})/(e^*_{100}-e^*_{1000})$, e^*_{100} and e^*_{1000} being the void ratios on the 1D-NCL* (or intrinsic compression line, ICL using Burland's notation) at σ'_{ve} = 100 and 1000kPa. There is a limiting value of I_v that corresponds to a specific volume,

v=1 and these values are stated on the graph. The compression paths may tend to curve at very high pressures if they approach this limit.

The effects of structure are indicated by the degree to which the compression paths of the intact samples cross the ICL and these are most obvious in soils with higher in-situ values of void index (I_v). However, there is not much difference between the HDV and CDV, so the effects of weathering are not completely clear or consistent. The magnitude of the effect of structure is similar to that in low to medium sensitivity clays (Burland, 1990) and also quite similar to the effects of structure in granitic saprolites (Rocchi and Coop, 2015). The tendency of an apparently lower effect of structure for lower initial I_v values is also seen for sedimentary soils (e.g. Cotecchia and Chandler, 2000) and CDG (e.g. Rocchi and Coop, 2015). Gasparre and Coop (2008) highlighted this as an artefact of the I_v normalisation rather than necessarily a true indication of the quantitative effects of structure, which may be more apparent in shearing (e.g. Hosseini Kamal et al., 2014).

After yield the compression curves of the intact samples generally tend to converge back towards the ICL, indicating that the structure is being broken down by straining. In some cases, the convergence is complete at the highest stresses reached, indicating a complete breakdown of structure; in a few cases the paths for the intact samples move back across the ICL, which is only a feature that arises from fitting a straight ICL through the compression paths of the reconstituted samples which are in fact slightly convex, in contrast to the slightly concave paths found by Burland (1990) for clays. In some other cases the convergence is slower and the stresses applied have not been high enough to see this post-yield convergence, while for some of the densest samples the stresses were not even large enough to see a clear yield.

An attempt was also made to quantify these effects of structure using the stress sensitivity (S_σ) defined by Cotecchia and Chandler (2000) as the stress at yield (σ'_y) divided

by that on the ICL at the same *v*. A modified stress sensitivity called pseudo-stress sensitivity ($S_{\sigma,10}$) was also used, obtained in the same way but at a stress of 10 times yield stress. Finally, the swell sensitivity (S_s) (Schmertmann, 1969), was quantified. This is the ratio of the gradients of the swelling lines of the reconstituted soil and the intact. The various sensitivities are shown in Figure 13(b, c & d). For S_σ, almost all the samples show positive effects of structure with no particular trend with depth or degree of weathering, apart from the shallow HDG samples giving high values. For $S_{\sigma,10}$, the data are still scattered but a clearer trend of reduction in the effects of structure with weathering, as might be expected can be seen. In contrast, the values of S_s are all close to unity indicating that the effects of structure are small.

6. SHEARING BEHAVIOUR

Typical stress-strain behaviour of the reconstituted and the intact samples from undrained and drained triaxial tests are shown in Figures 15 and 16. Details of the tests are given in Table 2; the labels indicate the location with the first letter, followed by the weathering degree and mean effective stress, p', at the beginning of shearing, then type of test (drained/undrained) and finally R stands for reconstituted while no letter is used for the intact samples. For undrained tests, the changes in pore pressure (Δu) have been normalised by the mean effective stress prior to shearing (p_0').

The stress-strain behaviour is related to both the stress level and initial v as well as the type of loading, but for most of the tests the deviatoric stress (q) increases monotonically with axial strain (ε_a) to a well-defined critical state, with only a few intact samples giving well-defined peaks. The pore pressure changes as well as the volumetric responses were positive

362 and so the behaviour of both the intact and reconstituted samples can be said to be generally
363 strain hardening and contractant.

364 The stress paths and critical states are shown in the q: p' plane in Figure 17. While all
365 the critical states are shown, only a few representative stress paths are shown for clarity. The
366 reconstituted samples are shown with broken lines and grey or black represent different
367 locations or weathering degrees while the intact samples are shown by chained dotted lines.
368 The critical states are represented by solid and empty markers for reconstituted and intact
369 samples respectively. The gradients of the critical state lines (M) vary only slightly for different
370 weathering degrees and the average value has been represented by a line in Figure 9(d). It is
371 clear that the variability of M is much less than those of the compressibility parameters, λ and
372 N_0. However, when analysed in terms of grading, as in Figure 10(d), M can be seen to reduce
373 with increasing fines, as would be expected. The value of M therefore tends to increase slightly
374 with depth and reduced weathering, as can be seen in Figures 9 and 18. Also, when analysed
375 in terms of mineralogy as shown in Figure 12(a & b), there seems to be a good correlation as
376 represented by the regression lines, M reducing as clay the minerals increase and the quartz
377 decreases. The critical state angle of shearing resistance (φ'_{cs}) values range from 31^0 for most
378 the weathered soils (ewCDV) to 37^0 for least weathered soils (wmwHDV).

379 In comparison with other similar soils, for a single Hong Kong CDV, Wang and Yan
380 (2006) obtained an M value of 1.48, corresponding to 36.6^0; for the Hong Kong granitic
381 saprolites, Rocchi and Coop (2015) obtained M values of 1.28-1.53, corresponding to 31.8-
382 37.5^0, which also tended to decrease with weathering. For a Brazilian residual soil from
383 gneissic rock, Futai et al. (2004) obtained slightly lower M values of 1.01-1.36 corresponding
384 to $25.6\text{-}33.7^0$. It is interesting to see that despite the different parent rocks, gradings and origins
385 from different parts of the world, these properties are relatively similar. Futai et al. (2004) and

386 Rocchi and Coop (2015) found peak strengths for their soils but for this research, generally
387 peaks were not observed and the deviatoric stress rises monotonically to the critical state. Only
388 two tests give slight peaks that plot very close to the critical state strengths in Figure 17(f).

389 Figure 19 presents the behaviour of the soils during isotropic compression and
390 subsequent shearing in the triaxial tests in the volumetric plane. The isotropic compression
391 stages for the reconstituted and intact samples are represented by short broken and long broken
392 lines respectively, shearing by solid lines and the critical states by solid and empty symbols for
393 the reconstituted and intact samples with black or grey for various weathering degrees. The
394 1D-NCL* have been added assuming a constant k_0 for each equal to (1-sinφ'). Since these cover
395 a much wider range of stress their gradients in the v:lnp' planes are useful to guide choice of
396 the isotropic normal compression lines for the reconstituted samples (NCL*), for which the
397 data cover a much narrower range, assuming them to be parallel. The critical state data are
398 slightly scattered, arising from the accuracy achieved in the values of v. The discrete nature of
399 the points and the narrower stress range, means that it is difficult to choose a critical state line,
400 CSL, and these have again been assumed parallel to the 1D-NCL*. The critical state lines for
401 the reconstituted soil, CSL* and the intact, CSL, are in most cases the same, which indicates
402 that shearing was able to destructure the intact fabric completely, but in two cases (A ewCDV
403 and D wmwHDV) this has not been the case and the two lines are significantly offset which
404 may be a result of the low in-situ specific volumes of the intact samples compared with the
405 reconstituted samples. The spacing between the isotropic NCL*, 1D-NCL* and CSL* varies
406 significantly but not systematically for different weathering degrees.

407 Figure 20 summarises the CSL* in the volumetric plane for all the weathering degrees.
408 The most weathered soils again generally plot above the less weathered. The CSL* intercepts
409 at 1kPa (Γ) are plotted against depth in Figure 9(e), which indicates a reduction with depth for
410 the CDV, although the shallow HDV samples again lie outside the trend for the other data.

411 Figure 9(f) shows how far the in-situ states are from the CSL in terms of specific volume. The
412 state parameter ψ (Been and Jefferies, 1985; Wroth and Basett, 1965) was used and it indicates
413 that the in-situ states of the soils are all on the dry side of the CSL, so they would all be dilative
414 in shearing. Any trend with depth or degree of weathering is not clear, and neither the state
415 parameters nor the critical state line locations show excessive scatter despite the samples being
416 taken from numerous locations.

417 An attempt was made to normalise the shearing data for volume to derive state
418 boundary surfaces, which can help identify to what extent the intact structure influences the
419 shear strength, once any differences in density between the intact and reconstituted samples are
420 accounted for. Figure 21 presents examples of the normalised shearing behaviour for selected
421 weathering degrees. The stress paths were normalized with respect to equivalent pressures
422 taken on the intrinsic critical state line ($p'_{cs} = \exp(\frac{\Gamma - v}{\lambda})$) and also the critical state line gradient
423 (M). The critical states should then ideally plot at coordinates (1:1). The data are scattered,
424 largely as a result of the difficulty in achieving highly accurate values of v in these
425 heterogeneous soils, but tentative intrinsic state boundary surfaces (SBS*) may be identified
426 from the shearing data for reconstituted samples. In common with other well graded residual
427 soils such as granitic saprolites (e.g. Rocchi and Coop, 2015) or residual sandstones (Ferreira
428 & Bica, 2006) the CSL lies to the left of the apex of the SBS*. The number of intact samples
429 that could be tested was quite limited because of the extreme difficulty of trimming the samples
430 successfully, so there are few data, but for the vwwHDV it is clear that the structure of the
431 intact sample does not give rise to any additional strength. For the ewCDV, this is less clear
432 because the difference in densities of the intact and the reconstituted samples that could be
433 made are quite different, so the data do not overlap. Nevertheless, since the SBS* must continue
434 from the CSL towards the origin with values of q/p' that must be above M (i.e. a gradient of

435 1.0 on this plot), it is unlikely again that the intact sample stress paths could rise significantly
436 above the SBS*, indicating that the effect of structure on strength is small or absent.

437 Figure 22(a & b) presents the shear stiffnesses for the reconstituted and intact samples
438 obtained from the vertical bender element measurements (G_{vh}). The normalisation for volume
439 has been made using a void ratio function ($f(e)=e^{-1.3}$) proposed by Jamiolkowski et al. (1991).
440 In each case the elastic shear modulus increases with p' as expected, but no clear trend with
441 weathering degree can be seen, which was a feature also seen for the granitic saprolites by
442 Rocchi and Coop, (2015). The stiffnesses are also similar in value to those soils. After
443 accounting for differences of void ratio, the stiffnesses of the intact samples do not plot above
444 those of the reconstituted in Figure 22b, indicating no clear effect of structure also at small
445 strains in shearing. Both horizontally and vertically orientated bender elements were also used
446 in lateral T-elements (Pennington *et al*., 1997), measuring the stiffnesses in the vertical plane
447 G_{hv} and the horizontal, G_{hh}. In Figure 23 the ratio of the two is used to quantify the degree of
448 anisotropy, which varies around 1.0, with some scatter, indicating no strong anisotropy for
449 either the reconstituted or intact samples, confirming the SEM observations.

450

451 **7. CONCLUSIONS**

452 The evolution of the physical properties, mechanical behaviour and geological structure of
453 volcanic saprolites with varying weathering degrees, from different locations and belonging to
454 two formations have been studied in reconstituted and intact states. The extreme heterogeneity
455 of the soils leads to significant scatter, which will reflect spatial variability due to the variability
456 of weathering and differences in the parent rocks. Nevertheless, trends were observed which
457 can be summarised as follows.

458 Weathering causes changes both to the intrinsic behaviour of the soils and also to the
459 effects of the structure. For the intrinsic behaviour, as the degree of weathering increases

towards the surface, the grading becomes generally finer and better graded, with an increased clay mineral content. The weathering generally causes a reduction in the angle of shearing resistance (φ'_{cs}) or the critical state line gradient (M) and an increase in the intrinsic compressibility of the soils. However, there is no effect of the weathering on the shear stiffnesses of the reconstituted samples and the degree of anisotropy is low in all cases.

The weathering causes the in-situ specific volumes to increase, but applying normalisations to compare the behaviour of intact samples with the intrinsic behaviour from reconstituted samples, the effects of structure are small to medium in compression. An analysis of the stress sensitivity at ten times the yield stress showed that the effect of structure tends to reduce with weathering. In contrast, there is no significant effect of structure in shearing at small or large strains. Overall, the effects of weathering on both the intrinsic properties and the structure were very similar to those seen by Rocchi and Coop (2015) for the granitic saprolites also from Hong Kong. Within the scatter of the data, the differences between two formations of volcanic saprolites tested were small, as were the differences between different locations.

The SEM images indicated that there was no strong anisotropy either in the reconstituted or intact samples and this was confirmed using multi-directional bender elements.

ACKNOWLEDGEMENTS

This work was fully supported by a grant from the Research Grant Council of the Hong Kong Special Administrative Region (HKSAR), China (T22-603/15N). The authors would also like to thank the Research Grant Council of the Hong Kong Special Administrative Region (HKSAR), China for the award of the Hong Kong PhD Fellowship Scheme (HKPFS) to the student for his PhD programme which led to this paper.

NOTATION

B coefficient of saturation

C_c compression index

CF clay fraction

C_u coefficient of uniformity

C_s*, C_s swelling index for reconstituted and intact soil respectively

D_{50} mean particle size

e_0 initial void ratio

G elastic shear stiffness

I_v void index = $(e-e_{100})/(e_{100}-e_{1000})$

LL liquid limit

M critical state gradient (q/p')

N_0 1D-NCL* intercept at 1kPa

PI plasticity index

PL plastic limit

p' mean effective stress

p_0' mean effective stress prior to shearing

p'_{cs} equivalent pressure taken on the CSL

q deviatoric stress

S_s swell sensitivity = C_s*/C_s

S_σ stress sensitivity = σ'_y/σ'_{ve}

$S_{\sigma,10}$ pseudo-stress sensitivity = $10*\sigma'_y/\sigma'_{ve}$

v specific volume

Δe change in void ratio

Δu change in pore water pressure

510 λ slope of 1D-NCL* taken as $C_c/2.303$

511 Γ intercept of CSL at 1kPa

512 ψ state parameter

513 σ'_v vertical effective stress

514 $\sigma'_{v\,insitu}$ in-situ vertical effective stress

515 σ'_{ve} equivalent vertical effective stress taken on 1D-NCL*

516 σ'_y yield stress

517 ε_a axial strain

518 ε_v volumetric strain

519 φ'_{cs} critical state angle of shearing resistance

520

521

522 **REFERENCES**

523 Alavi Nezhad Khalil Abad, S.V., Mohamad, E.T., Komoo, I., 2014. Dominant weathering
524 profiles of granite in southern Peninsular Malaysia. Eng. Geol. 183, 208–215.
525 http:// dx.doi.org/10.1016/j.enggeo.2014.10.019.

526 Alavi Nezhad Khalil Abad, S.V., Tugrul, A., Gokceoglu, C., Jahed Armaghani, D., 2016.
527 Characteristics of weathering zones of granitic rocks in Malaysia for geotechnical
528 engineering design. Eng. Geol. 200, 94–103.
529 http://dx.doi.org/10.1016/j.enggeo.2015.12.006.

530 Altuhafi, F., Coop, M. R., 2011. Changes to particle characteristics associated with the
531 compression of sands. Géotechnique 61, No. 6, 459-471.

532 Basu, A., 2015. Applicability of weathering classification to quartzitic materials and relation
533 between mechanical properties and assigned weathering grades: a comparison with
534 investigations on granitic materials. Engineering Geology for Society and Territory

volume 6. Springer, pp. 865–868.

Basu, A., Celestino, T.B., Bortolucci, A.A., 2009. Evaluation of rock mechanical behaviors under uniaxial compression with reference to assessed weathering grades. Rock Mech. Rock. Eng. 42, 73–93.

Been, K., Jefferies, M. G., 1985. A state parameter for sands. Géotechnique 35, No. 2, 99–112, http://dx.doi.org/10.1680/geot.1985.35.2.99.

Burland, J. B., 1990. On the compressibility and shear strength of natural clays. Géotechnique 40, No. 3, 329–378, http://dx.doi.org/10.1680/geot.1990.40.3.329.

Cafaro, F., Cotecchia, F., 2001. Structure degradation and changes in the mechanical behaviour of a stiff clay due to weathering. Géotechnique 51, No. 5, 441–453, http://dx.doi. org/10.1680/geot.2001.51.5.441.

Chandler, R.J., 1972. Lias clay: Weathering processes and their effects on shear strength. Géotechnique 22, No. 3, 403-431.

Cotecchia, F., Chandler, R. J., 2000: A general framework for the mechanical behaviour of clays. Géotechnique 50, No. 4, 431-447.

Ferreira, P. M. V., Bica, A. V. D., 2006. Problems in identifying the effects of structure and critical state line in a soil with a transitional behaviour. Géotechnique 56, No. 7, 445–454, http://dx.doi.org/10.1680/geot.2006.56.7.445.

Ferreira, C., da Fonseca, A. V., Nash, D. F. T., 2011. Shear wave velocities for sample quality assessment on a residual soil. Soils & Found. 51, No. 4, 683–692.

Futai, M. M., Almeida, M. S. S., Lacerda, W. A., 2004. Yield, strength and critical state behaviour of a tropical saturated soil. ASCE J. Journal of Geotechnical and Geoenvironmental Engineering 130, No. 11, 1169–1179.

Gasparre, A., Coop, M. R., 2008. Quantification of the effects of structure on the compression of a stiff clay. Can. Geotech. J. 45, No. 9, 1324–1334.

560 GEO (Geotechnical Engineering Office)., 1988. Guide to rock and soil descriptions. Geoguide
561 3. Hong Kong: Geotechnical Engineering Office.
562 Hosseini-Kamal, R., Brosse, A., Coop, M. R., Jardine, R. J., 2014. The post-yield behaviour
563 of four Eocene-to-Jurassic UK stiff clays. Géotechnique 64, No. 8, 620–634,
564 http://dx.doi. Org/10.1680/geot.13.P.043.
565 Irfan, T. Y., 1996a. Mineralogy, fabric properties and classification of weathered granite
566 in Hong Kong. Quarterly Journal of Engineering Geology 29, 5-25.
567 Irfan, T. Y., 1999. Characterization of weathered volcanic rocks in Hong Kong. Quarterly
568 Journal of Engineering Geology 32, 317-348.
569 ISRM, 2007. In: Ulusay, R., Hudson, J. (Eds.), The Complete ISRM Suggested Methods for
570 Rock Characterization, Testing and Monitoring [1974–2006]. International Society of
571 Rock Mechanics.
572 Jamiolkowski, M., Leroueil, S., Lo Presti, D., 1991. Design parameters from theory to
573 practice. Geo-coast 1991: Proceedings of international conference on geotechnical
574 engineering for coastal development, Yokohama, Japan, pp. 877–917. Yokosuka City,
575 Japan: Port and Harbour Research Institute.
576 Lunne, T., Berre, T., Strandvik, S., 1997. Sample disturbance effects in soft low plastic
577 Norwegian clay. In Recent developments in soil and pavement mechanics (ed. M. S. S.
578 Almeida), pp. 81–102. Rotterdam, the Netherlands: Balkema.
579 Ng, C.W.W., Chiu, A.C.F., 2001. Behaviour of a loosely compacted unsaturated volcanic
580 soil. Journal of Geotechnical and Geoenvironmental Engineering 127, No. 12, 1027–
581 1036.
582 Pennington, D.S., Nash, D.F.T., Lings M.L., 1997. Anisotropy of G_o shear stiffness in
583 Gault clay. Géotechnique 47, No. 3, 391-398.
584 Rocchi, I., Coop, M.R., 2015. The effects of weathering on the physical and mechanical

properties of a granitic saprolite. Géotechnique 65, No. 6, 482-493, http://dx.doi.org/10.1680/geot.14.P.177.

Schmertmann, J.H., 1969. Swell Sensitivity. Géotechnique, 19, 530-533.

Shipton, B. J. I., Coop, M. R., 2012. On the compression behaviour of reconstituted soils. Soils & Found. 52, No. 4, 668–681.

Wang, Y.H., Yan, W.M., 2006. Laboratory studies of two Common saprolitic soils in Hong Kong. Journal of Geotechnical and Geoenvironmental Engineering 132, No. 7, 923-930.

Wroth, C. P., Bassett, R. H., 1965. A stress–strain relationship for the shearing behaviour of a sand. Géotechnique 15, No. 1, 32–56.

FIGURES

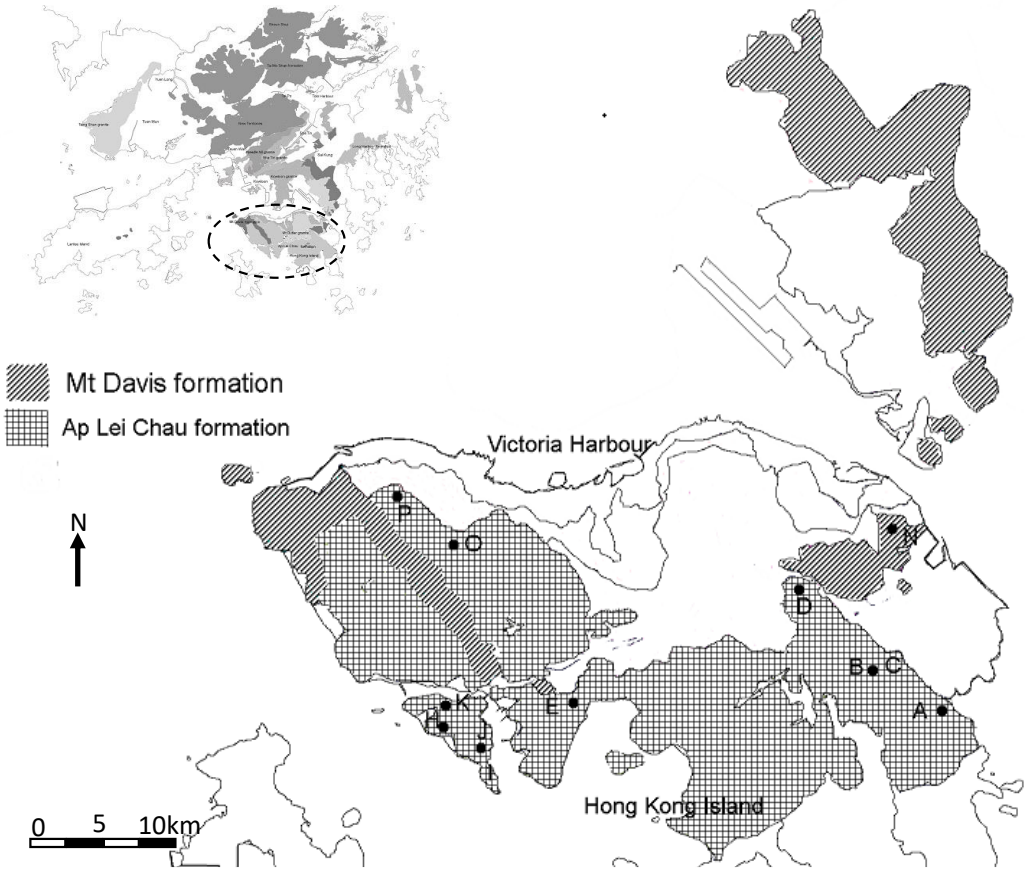

Figure 1: Map of sample locations.

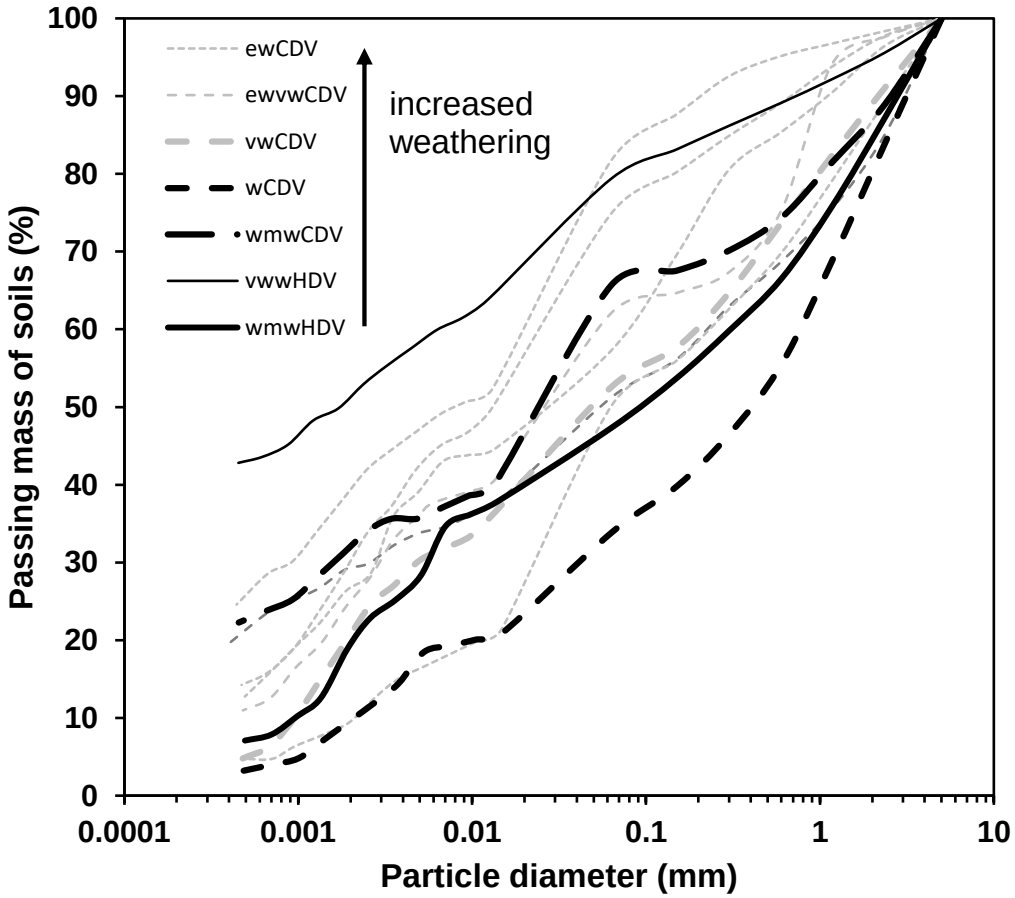

Figure 2: Grading curves for different weathering degrees

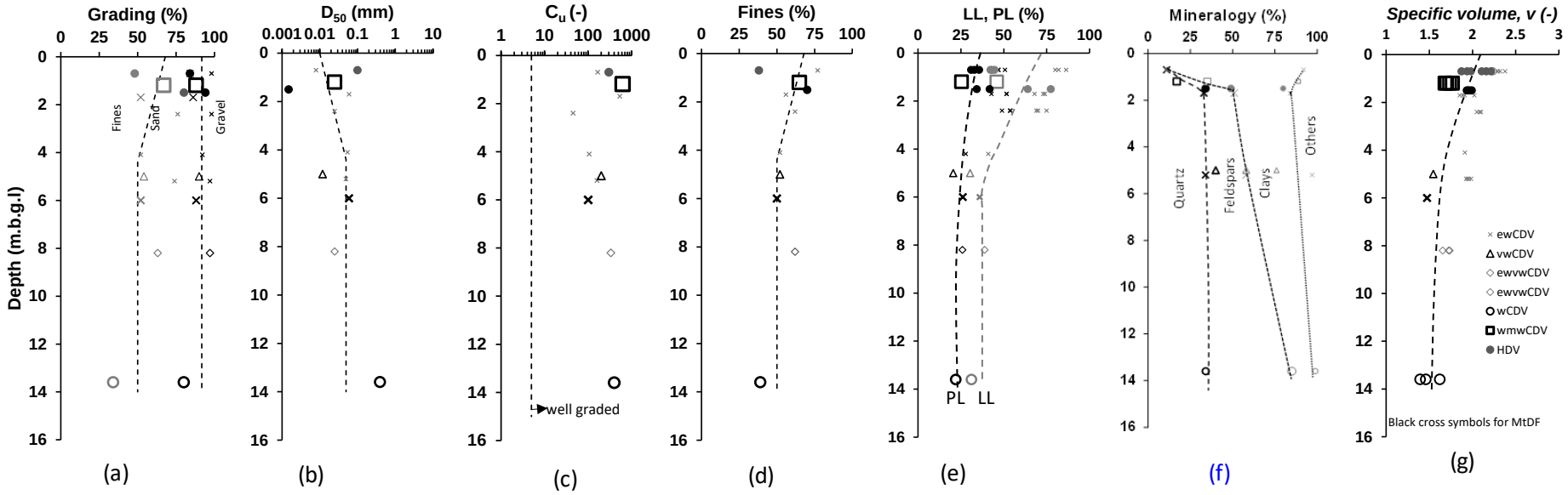

Figure 3: Profiles for the physical properties (MtDF mount Davis Formation)

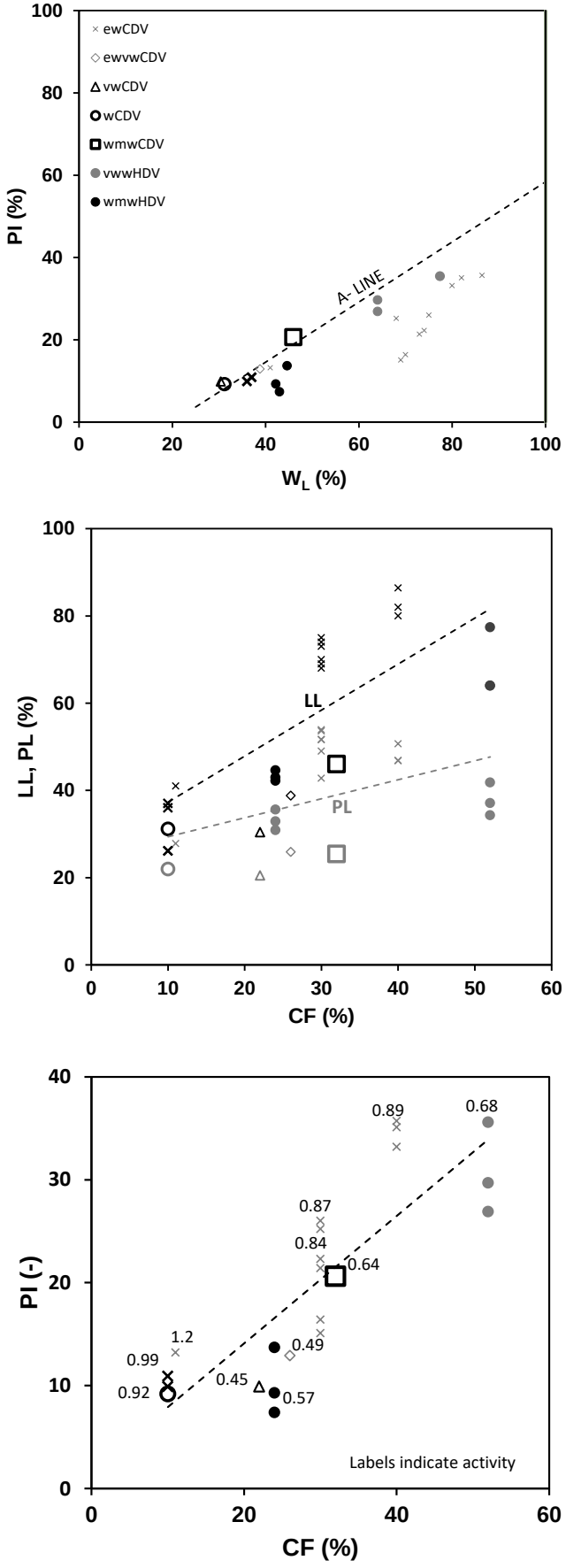

Figure 4: Index properties

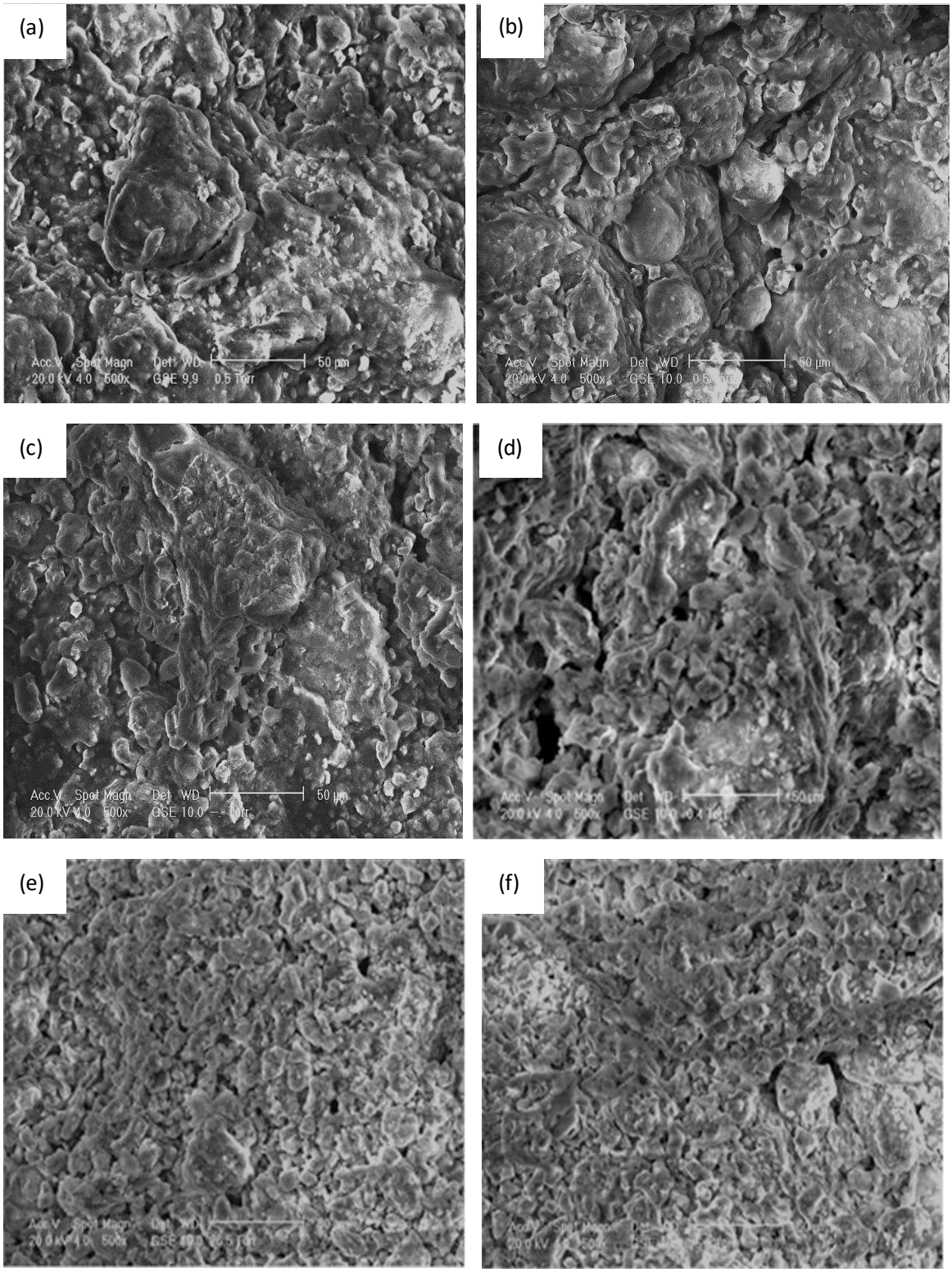

Figure 5: Microstructure of reconstituted samples: (a) B ewCDV horizontal plane (b) B ewCDV vertical plane (c) E vwwHDV horizontal plane (d) E vwwHDV vertical plane (e) P wCDV horizontal plane (f) P wCDV vertical plane. NB for vertical plane samples, vertical direction in SEM corresponds to vertical in the sample.

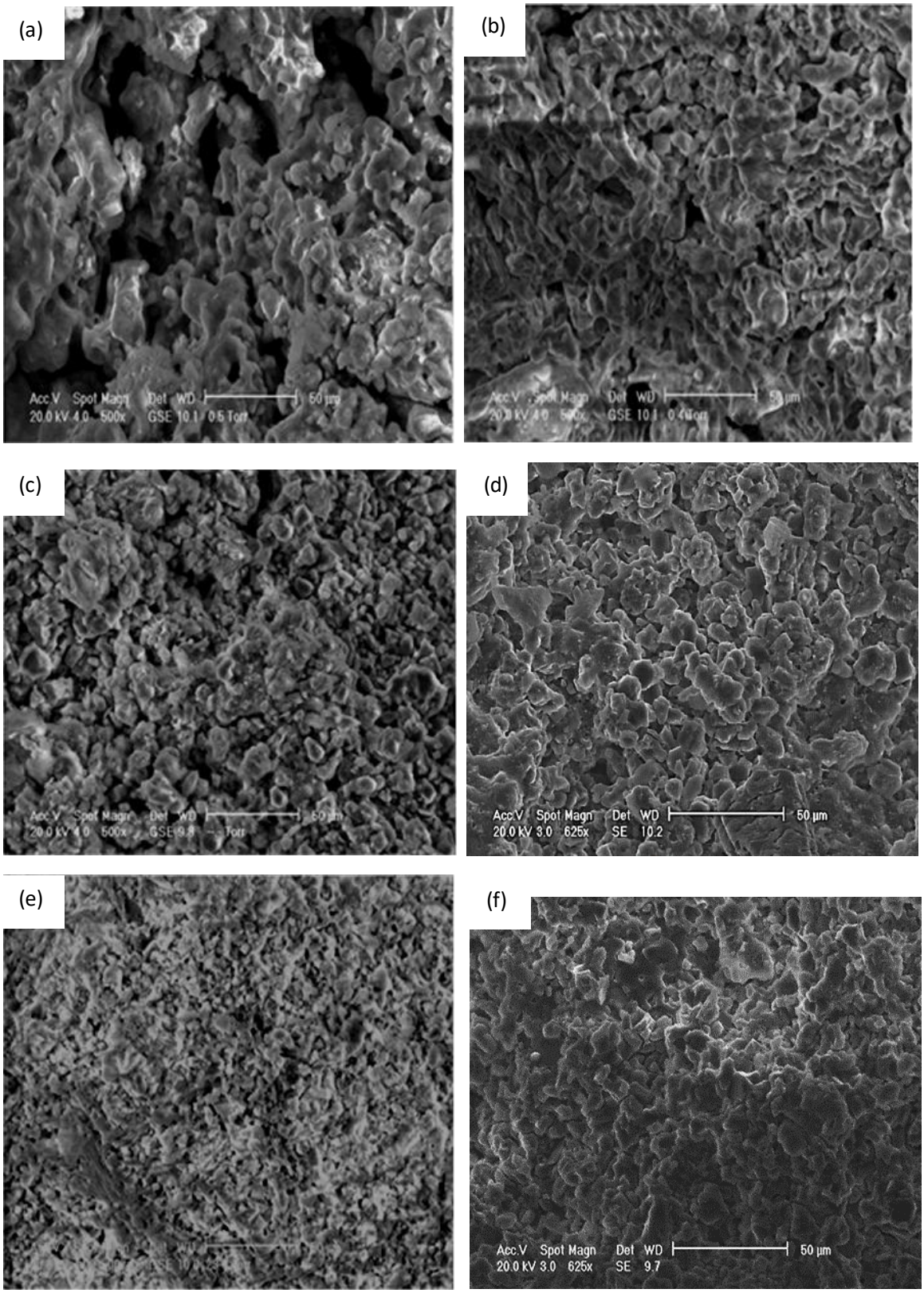

Figure 6: Microstructure of intact samples: (a) B ewCDV, (b) E vwwHDV, (c) sample J ewCDV horizontal plane, (d) J ewCDV vertical plane (e) P wCDV horizontal plane (f) P wCDV vertical plane.

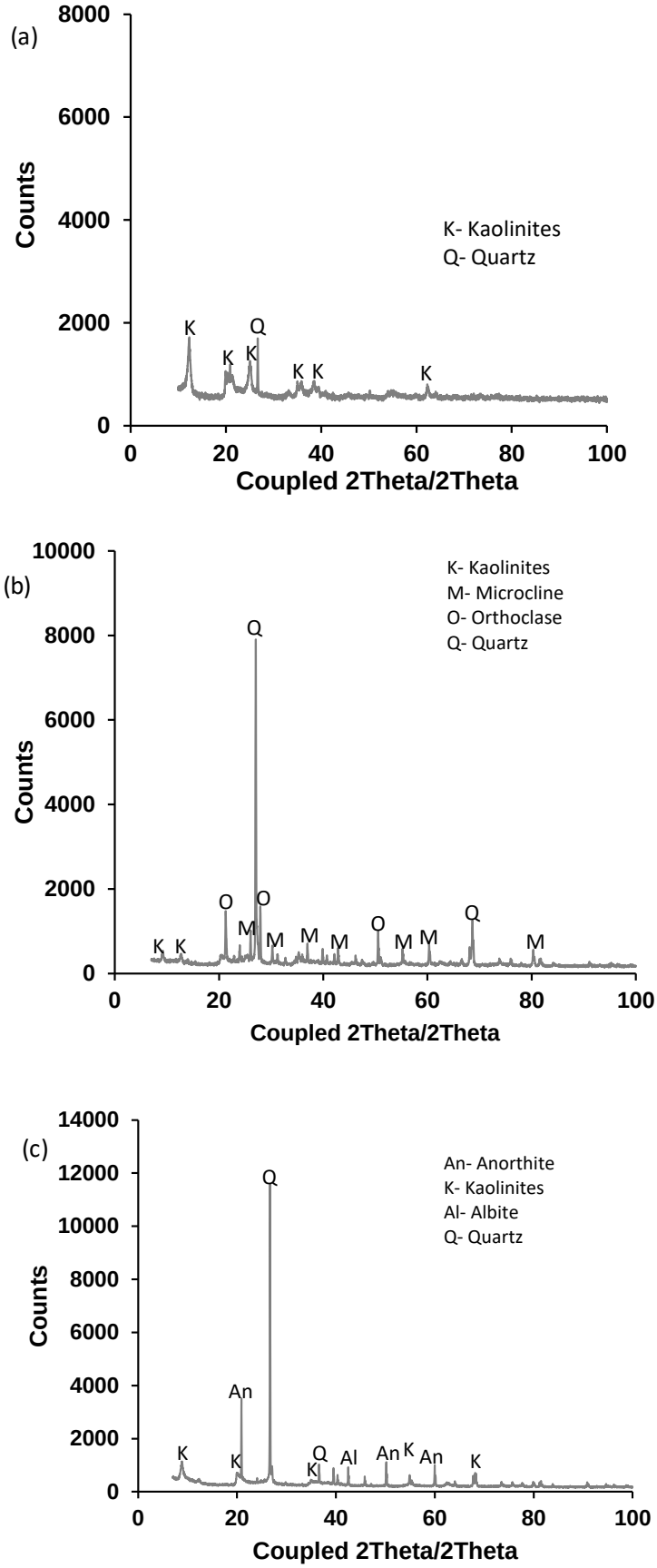

Figure 7: Mineralogy of selected samples: (a) A ewCDV, (b) P wCDV and (c) E vwwHDV

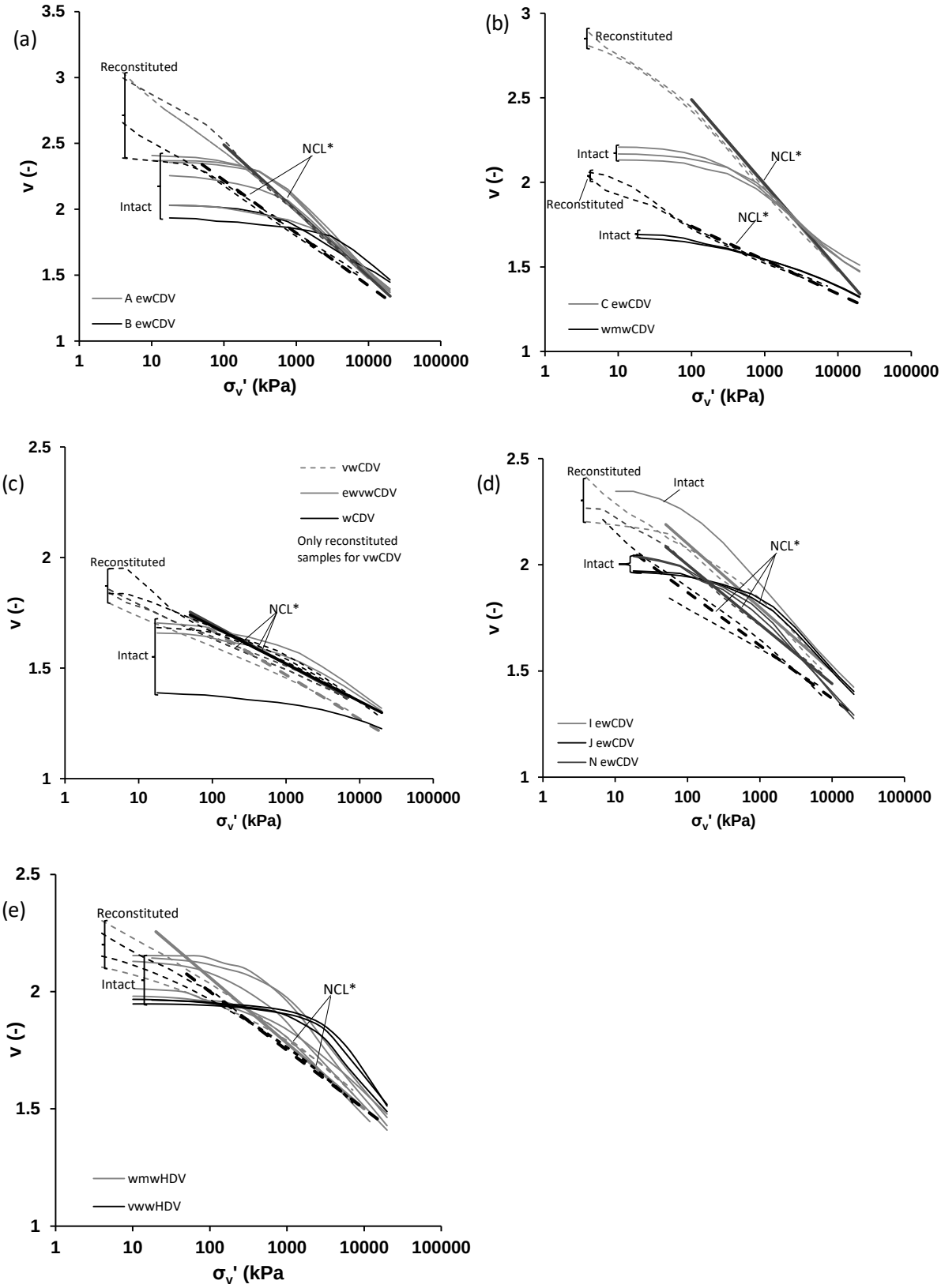

Figure 8: One-dimensional compression behaviour

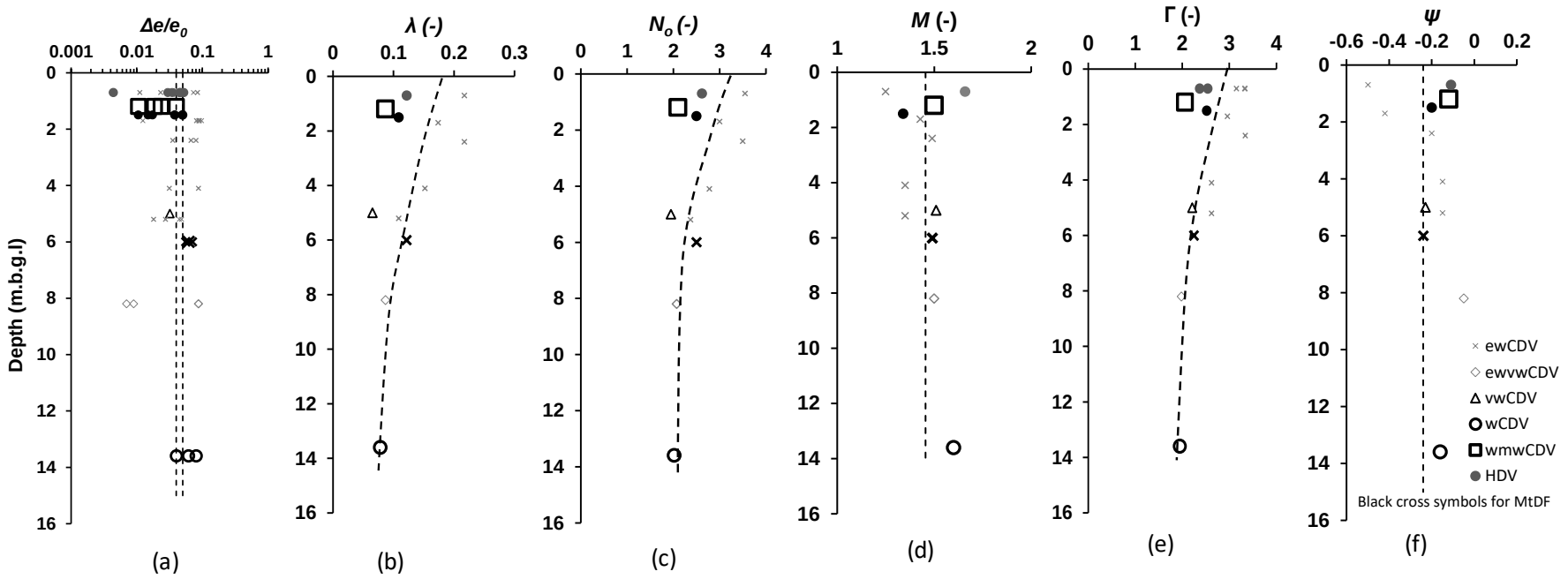

Figure 9: Profiles for the mechanical properties

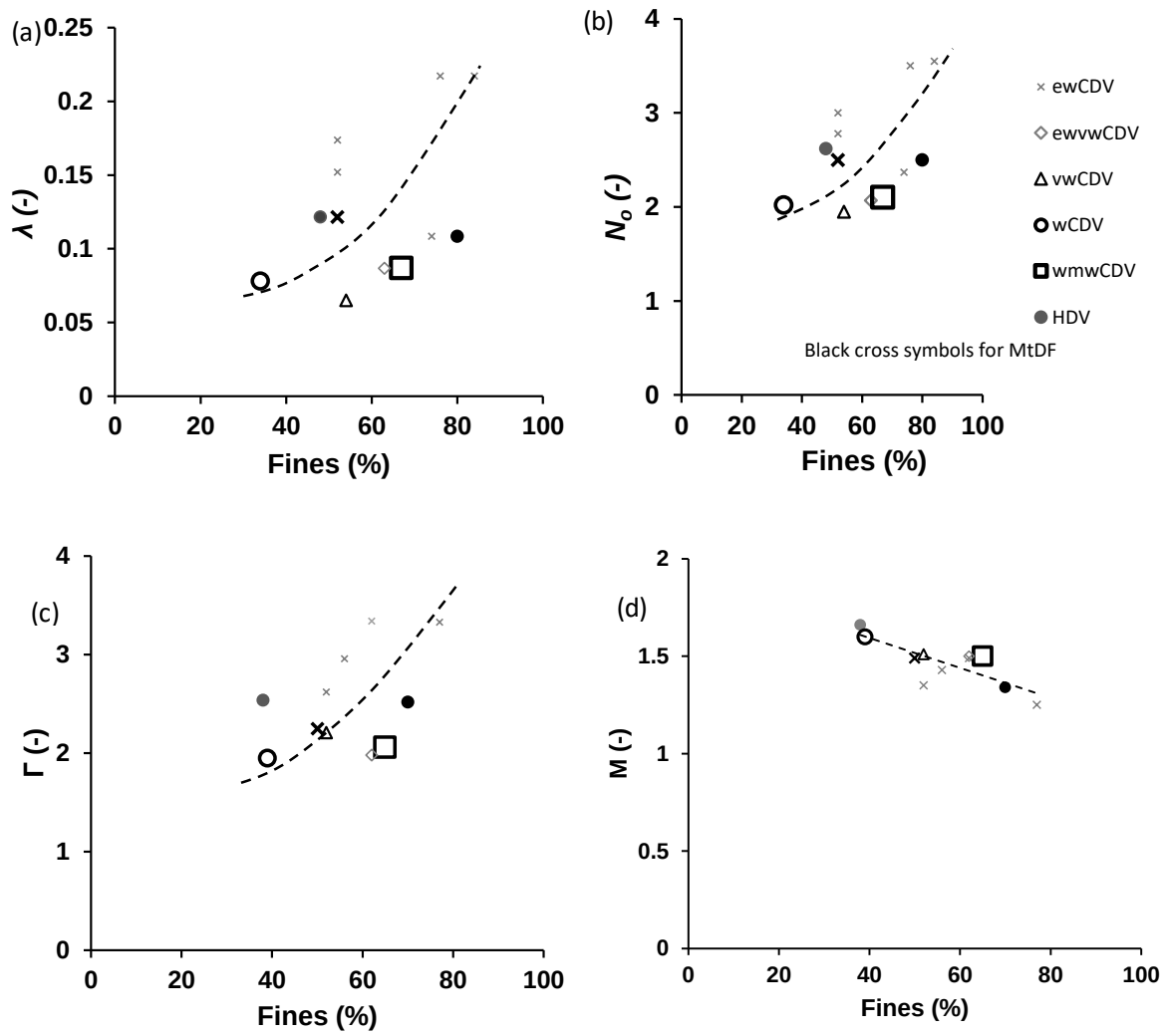

Figure 10: Variation of mechanical parameters with fines

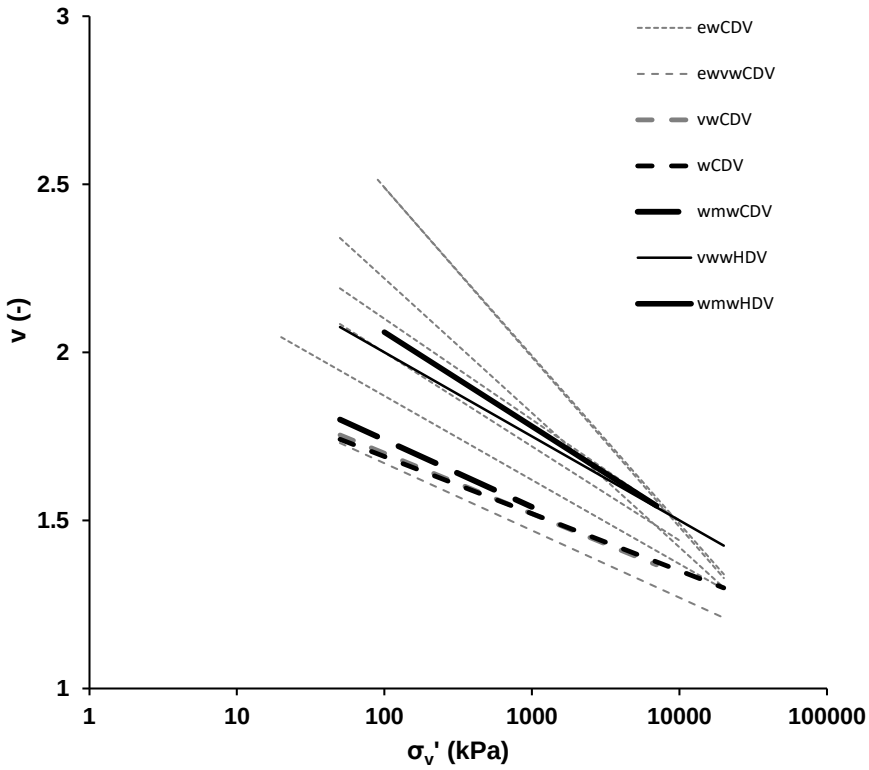

Figure 11: Summary of intrinsic normal compression lines

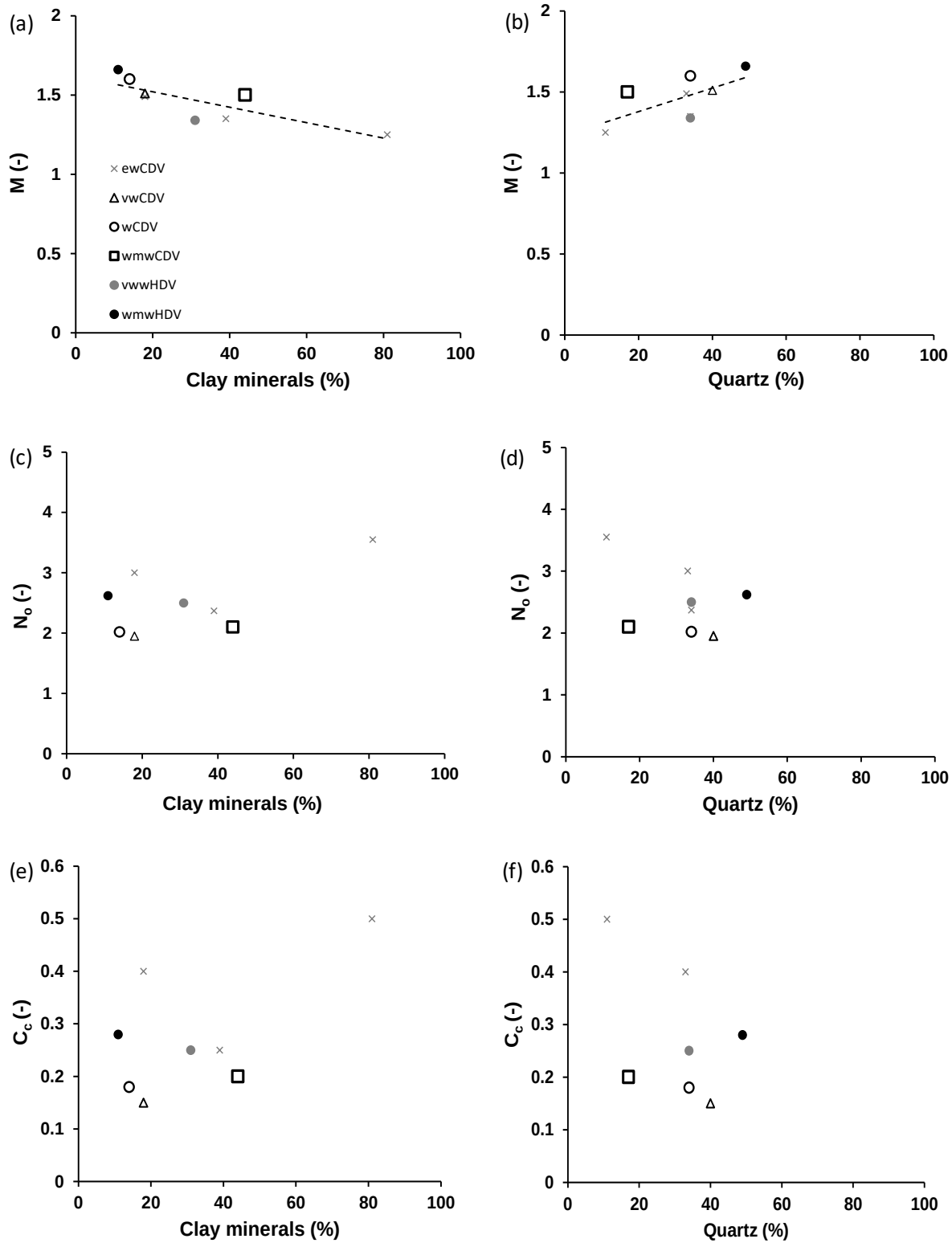

Figure 12: Variation of mechanical parameters with mineralogy

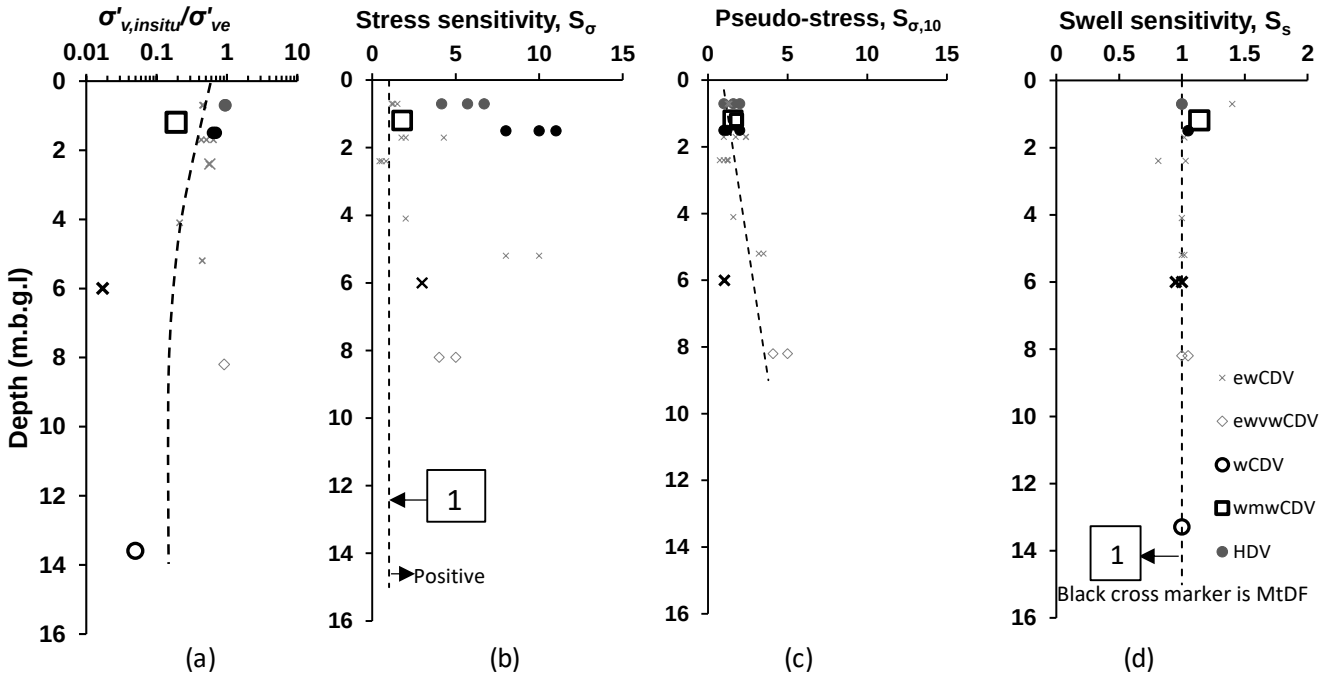

Figure 13: In-situ states and effects of structure

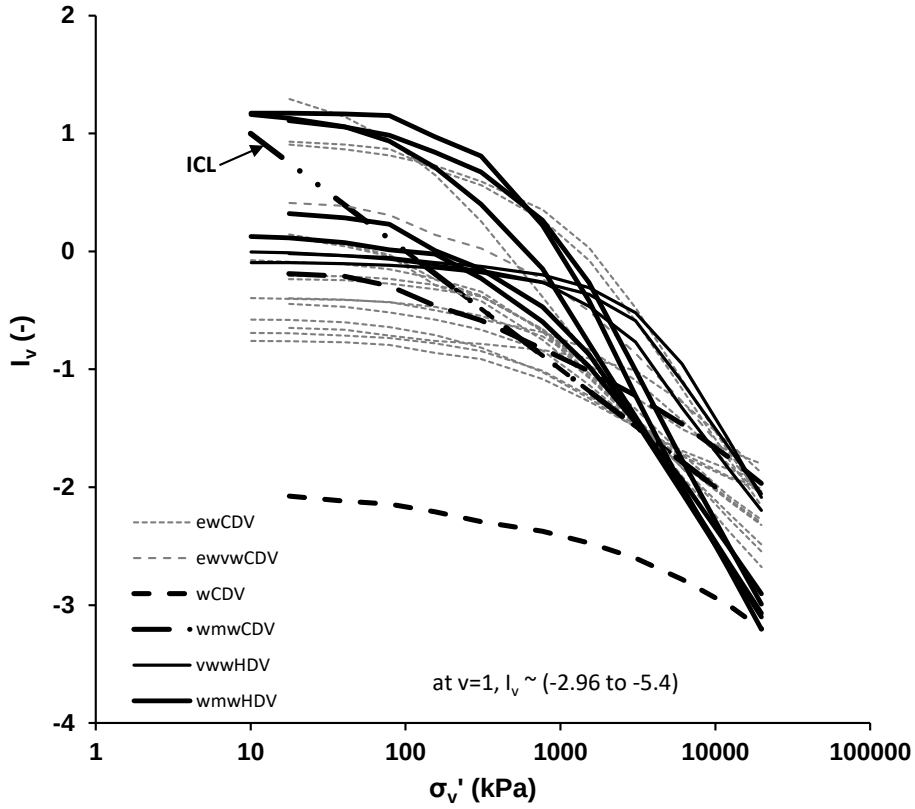

Figure 14: Normalised compression behaviour for the intact samples

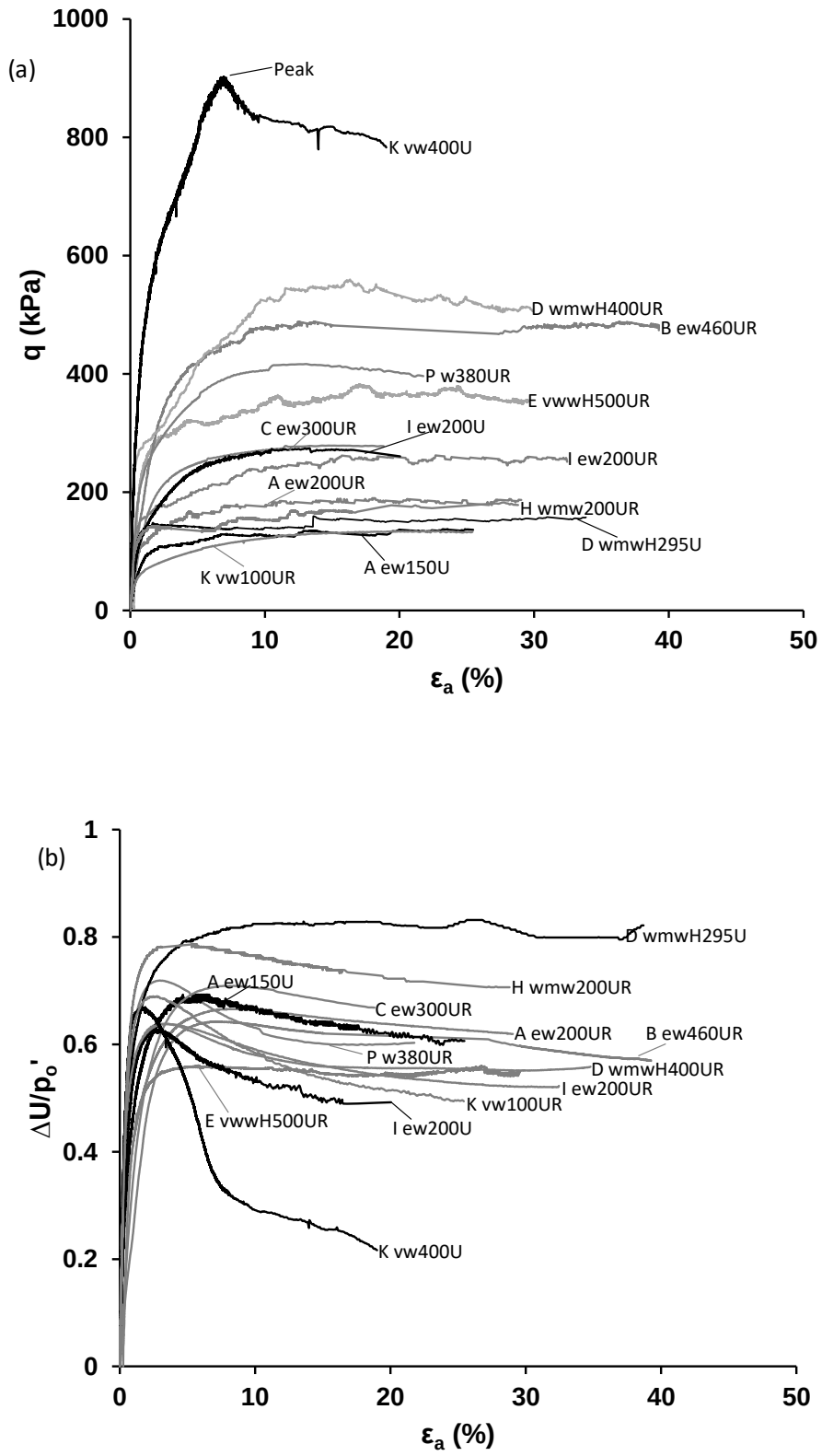

Figure 15: Stress-strain behaviour for undrained triaxial tests (grey reconstituted, black intact)

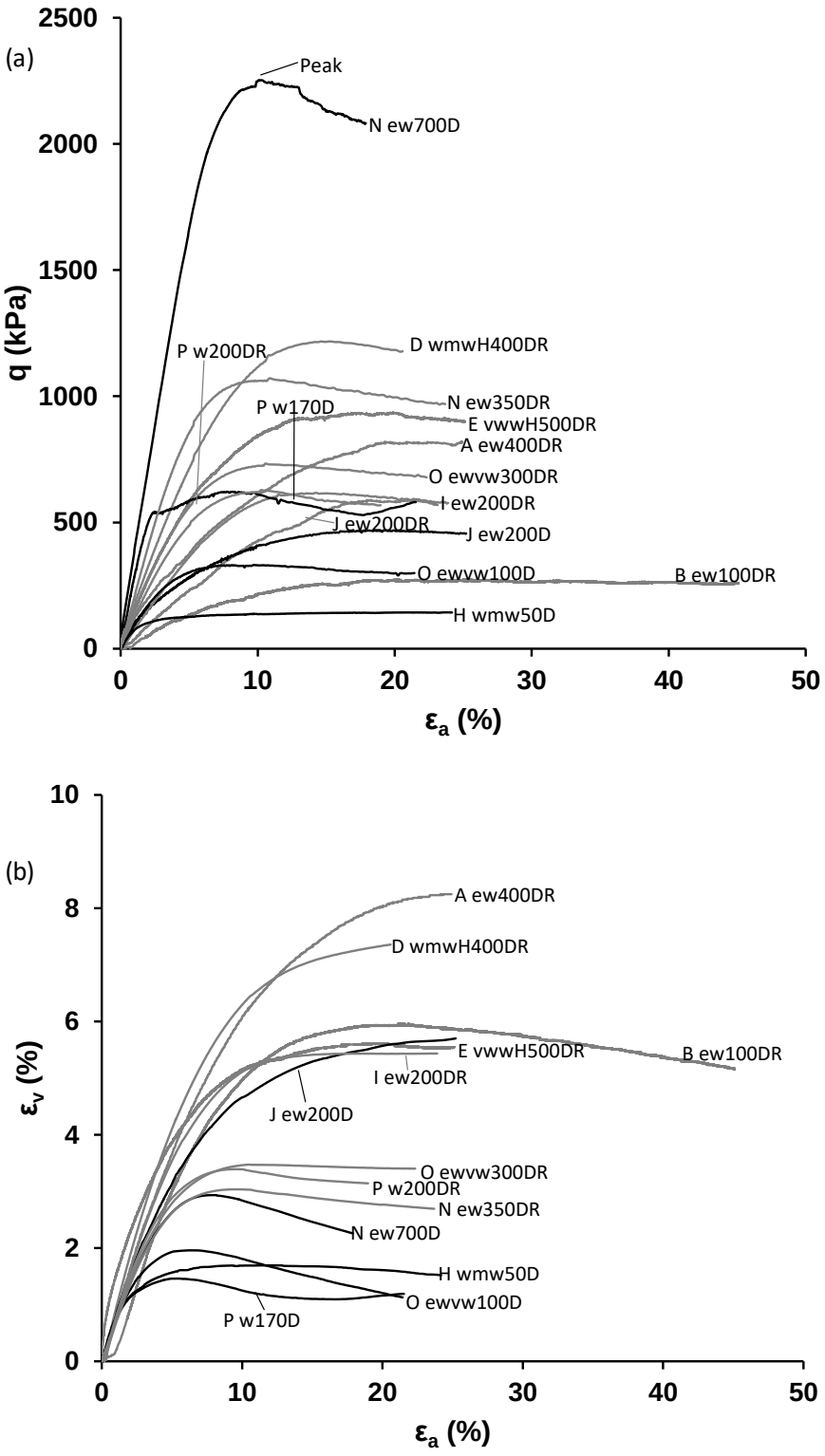

Figure 16: Stress-strain behaviour for drained triaxial tests (grey reconstituted, black intact)

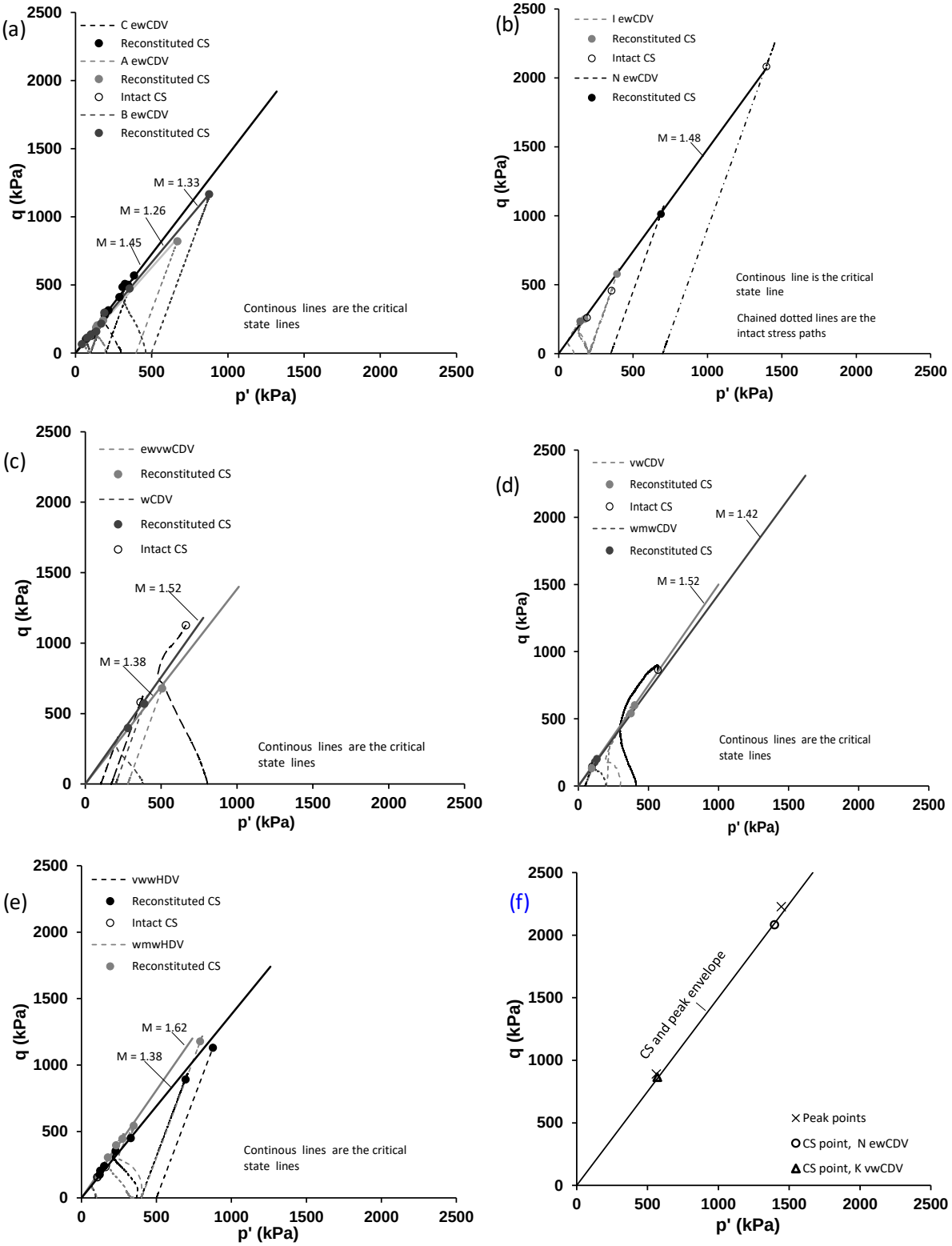

Figure 17: Stress paths, critical states and peak envelope

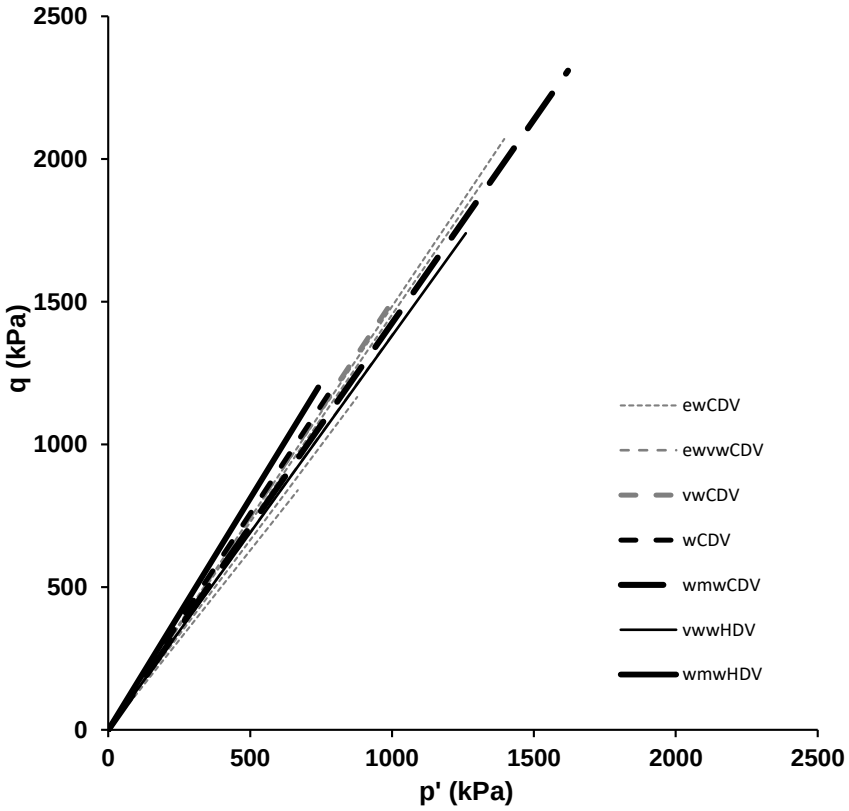

Figure 18: Summary of the critical state lines in the stress plane.

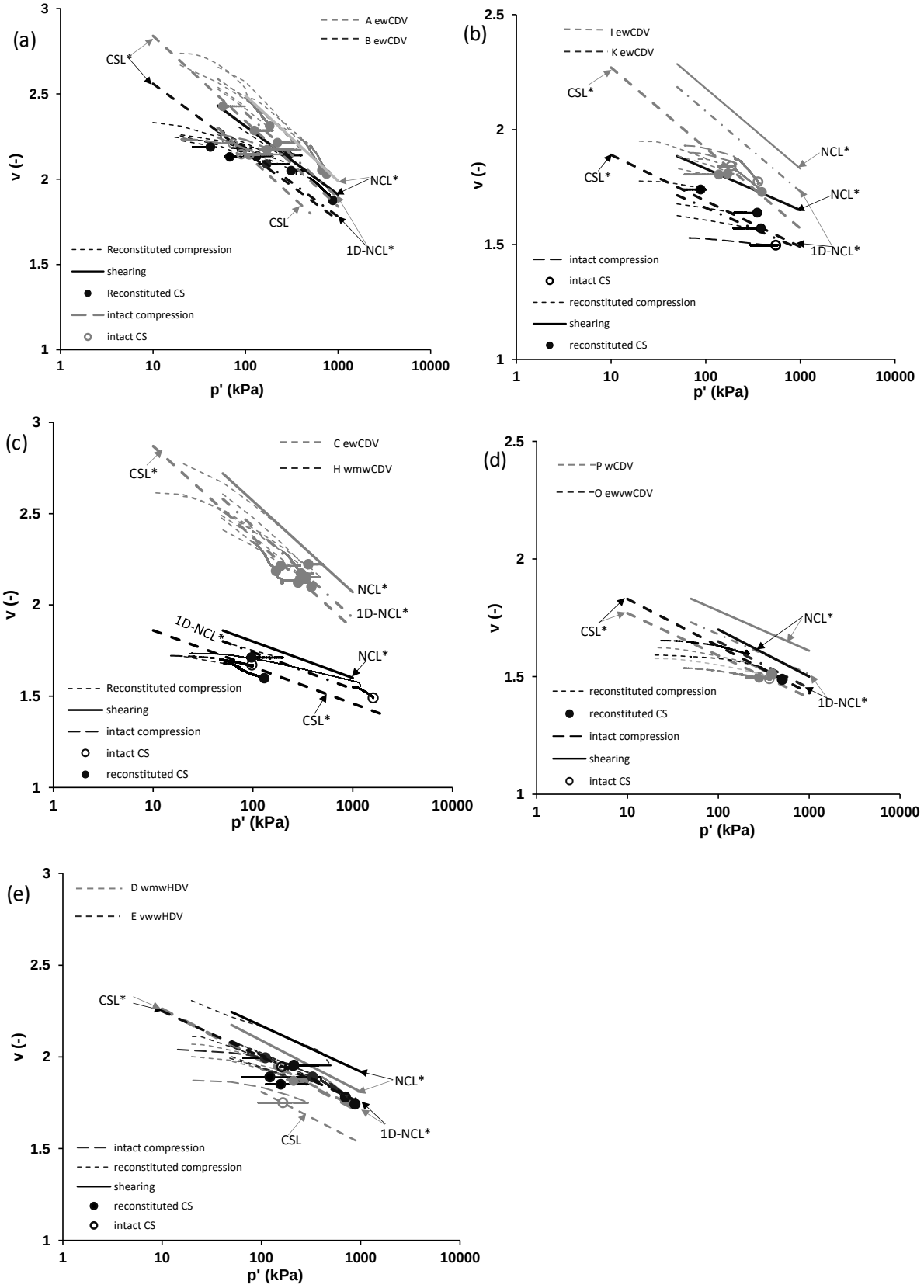

Figure 19: Behaviour in the volumetric plane

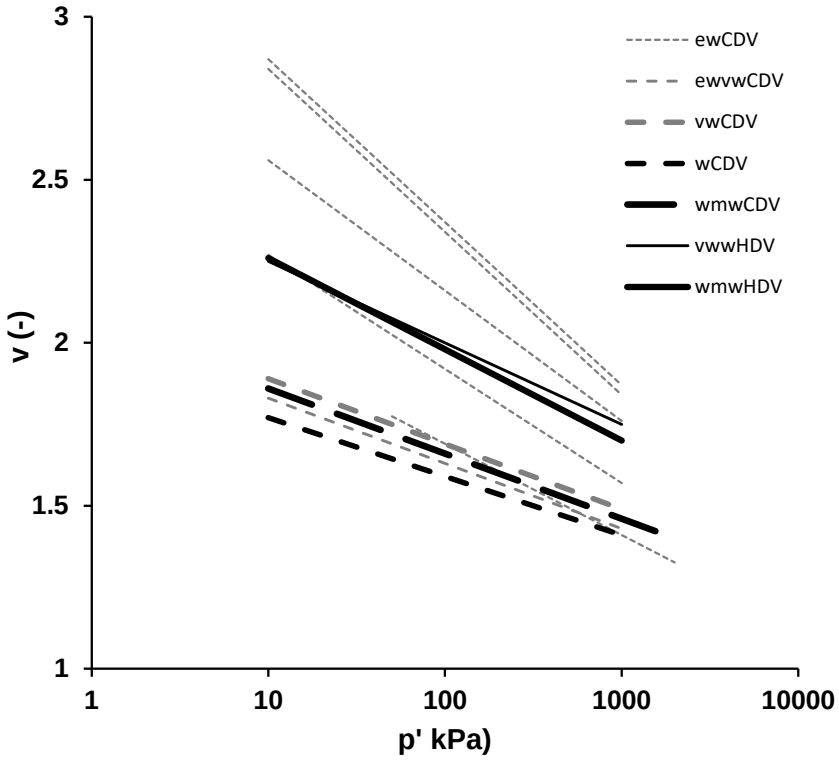

Figure 20: Summary of the critical state lines in the volumetric plane

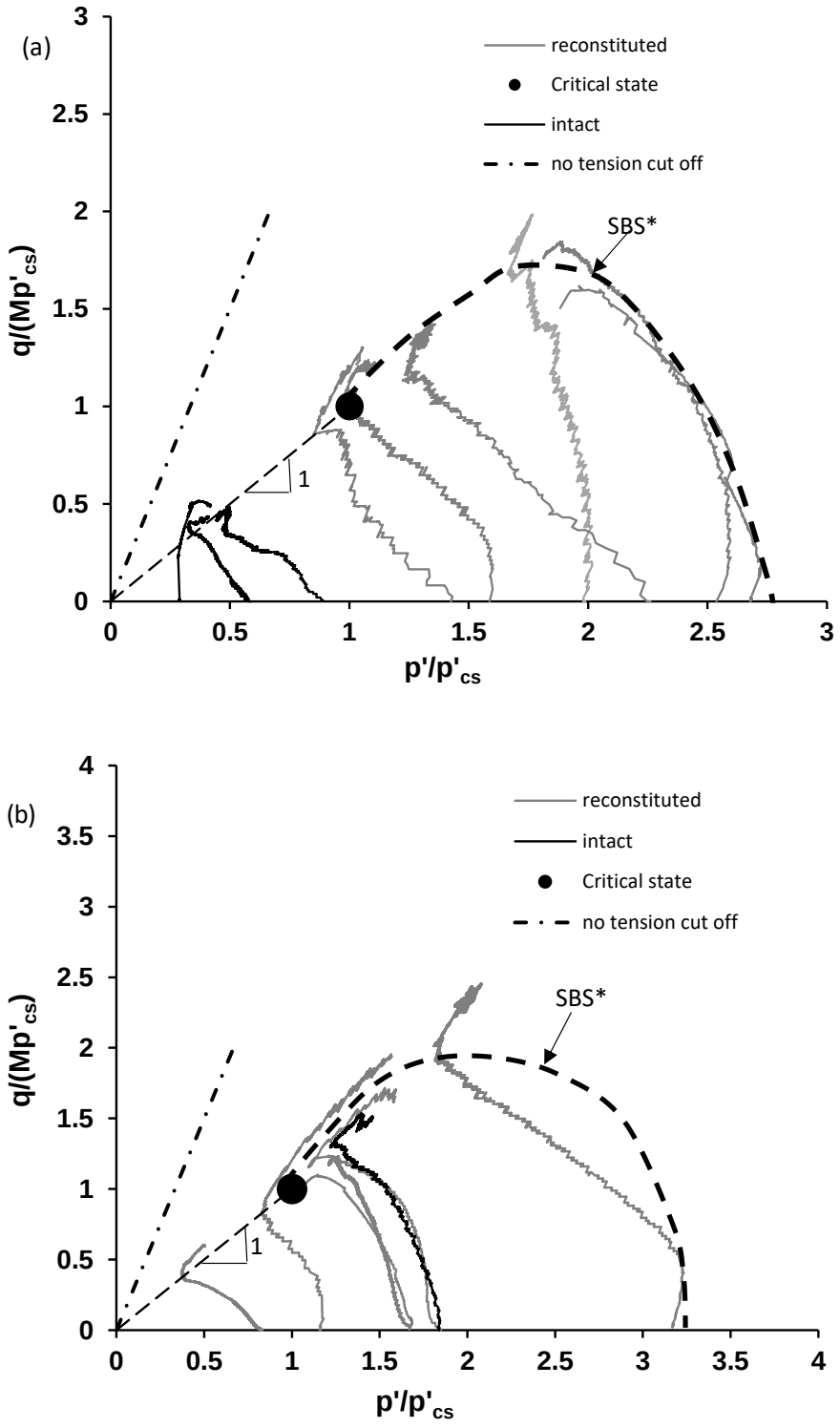

Figure 21: Examples of normalised shearing behaviour: (a) ewCDV and (b) vwwHDV

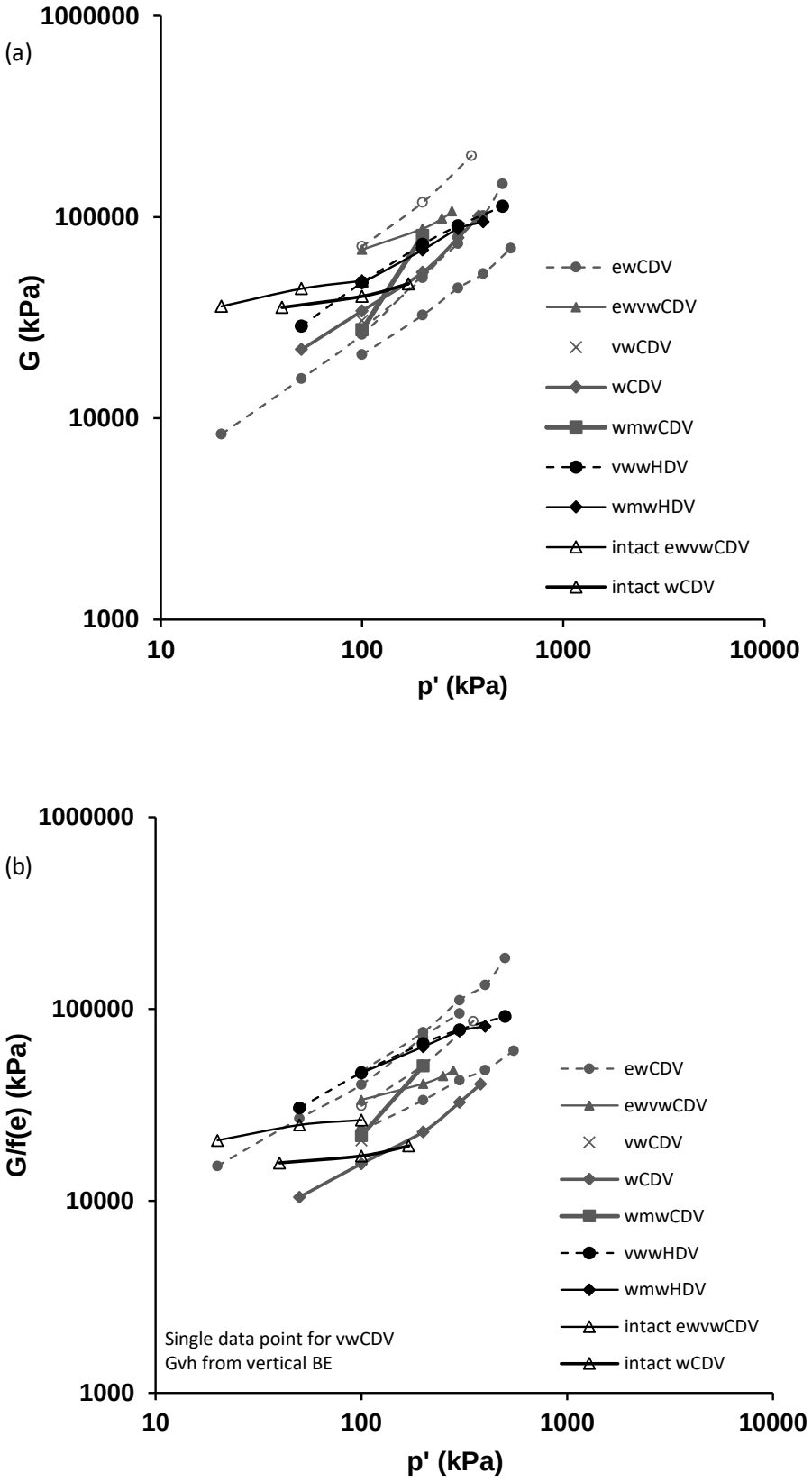

Figure 22: Normalised elastic shear stiffness behaviour

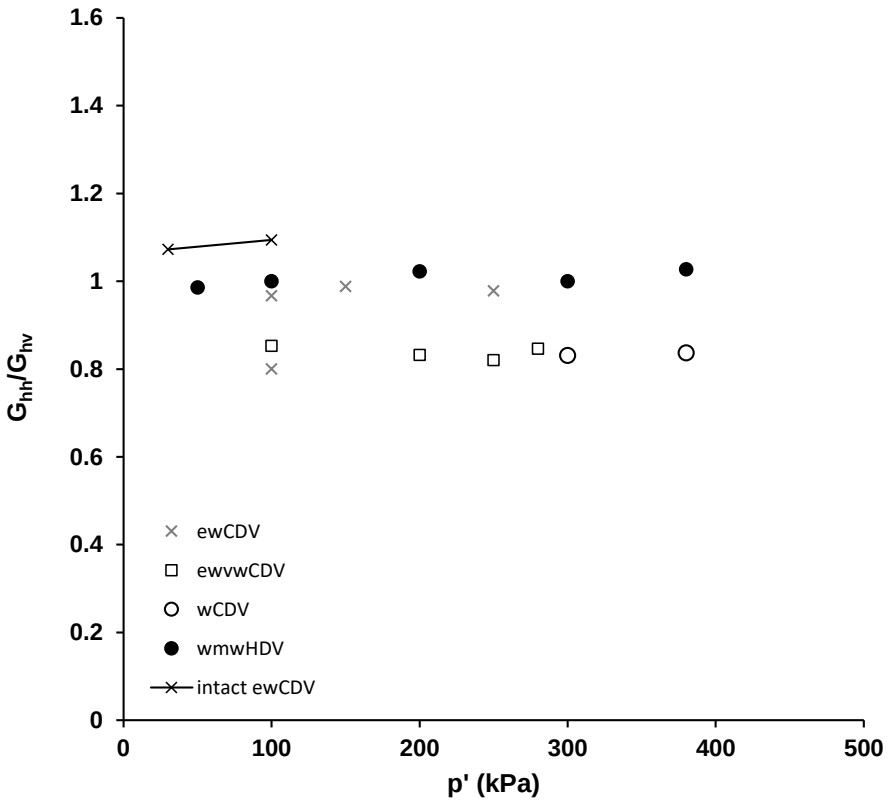

Figure 23: Anisotropic stiffness of the samples

TABLES

Table 1: Details of the sample tested

Location	Sample type/ borehole	Formation	Weathering degree	Depth (m)	Grading
A	Block	Ap Lei Chau	ewCDV	0.7-1	Fine
B	Block	Ap Lei Chau	ewCDV	1.7-2	Fine
C	Block	Ap Lei Chau	ewCDV	2.4-3.5	Fine
D	Block	Ap Lei Chau	wmwHDV	0.7-1	Fine
E	Block	Ap Lei Chau	vwwHDV	1.5-2.6	Fine
H	Mazier (DH1)	Ap Lei Chau	wmwCDV	1-1.4	Fine
I	Mazier (DH1)	Ap Lei Chau	ewCDV	3.6-4.6	Fine
J	Mazier (DH1)	Ap Lei Chau	ewCDV	4.7-5.7	Fine
K	Mazier (DH2)	Ap Lei Chau	vwCDV	4.5-5.5	Fine
N	Mazier (DH4)	Mount Davis	ewCDV	5.86-6.31	Coarse
O	Mazier (DH2)	Ap Lei Chau	ewvwCDV	8.10-8.35	Fine
P	Mazier (DH5)	Ap Lei Chau	wCDV	13.3-13.95	Fine

NB ew extremely weak, ewvw extremely weak to very weak, vw very weak, w weak, wmw weak to medium weak, vww very weak to weak, wmw weak to medium weak.

Table 2: Details of triaxial tests

Weathering degree	Test	v_o	p'_c (kPa)	v_c	Accuracy of v (+/-)	Sample/shearing condition
A ewCDV	A ew100UR	2.66	99	2.43	0.014	R/U
	A ew100DR	2.68	100	2.48	0.005	R/D
	A ew200UR	2.64	195	2.28	0.002	R/U
	A ew400UR	2.69	386	2.21	0.013	R/U
	A ew400UR1	2.67	397	2.17	0.005	R/U
	A ew400DR	2.68	400	2.23	0.003	R/D
	A ew500DR	2.73	500	2.19	0.02	R/D
	A ew50U	2.23	50	2.20	0.06	I/U
	A ew250U	2.28	250	2.14	0.003	I/U
	A ew150U	2.23	150	2.12	0.008	I/U
B ewCDV	B ew50UR	2.22	50	2.18	0.003	R/U
	B ew100UR	2.26	100	2.13	0.02	R/U
	B ew100UR1	2.32	100	2.17	0.07	R/U
	B ew200UR	2.30	200	2.13	0.07	R/U
	B ew300UR	2.33	300	2.11	0.01	R/U
	B ew460UR	2.27	460	2.02	0.02	R/U
	B ew500DR	2.23	498	1.97	0.001	R/D
	B ew550DR	2.23	550	1.91	0.03	R/D
C ewCDV	C ew100DR	2.58	100	2.34	0.07	R/D
	C ew200DR	2.59	199	2.28	0.04	R/D
	C ew300DR	2.59	298	2.21	0.02	R/D
	C ew345UR	2.57	343	2.13	0.003	R/U
	C ew395UR	2.46	394	2.12	0.01	R/U
	C ew400UR	2.72	396	2.17	0.03	R/U
	C ew475UR	2.61	474	2.15	0.01	R/U
	C ew500UR	2.77	500	2.22	0.012	R/U
D wmwHDV	D wmwH100DR	1.99	100	1.93	0.03	R/D
	D wmwH348UR	2.00	345	1.87	0.007	R/U
	D wmwH400DR	2.06	400	1.89	0.01	R/D
	D wmwH295U	1.87	295	1.75	0.004	I/U
E vwwHDV	E vwwH100UR	2.11	100	1.99	0.004	R/U
	E vwwH200UR	2.02	200	1.89	0.004	R/U
	E vwwH300UR	2.02	297	1.85	0.003	R/U
	E vwwH400UR	2.13	398	1.89	0.007	R/U
	E vwwH400DR	2.14	399	1.88	0.002	R/D
	E vwwH500DR	2.11	500	1.85	0.09	R/D
	E vwwH500UR	2.31	498	1.95	0.01	R/U
	E vwwH230U	2.04	230	1.94	0.04	I/U
H wmwCDV	H wmw50DR	1.71	50	1.67	0.002	R/D
	H wmw200UR	1.82	200	1.71	0.007	R/U
	H wmw50D	1.72	49	1.69	0.012	I/D
	H wmw100D	1.79	1000	1.59	0.017	I/D
I ewCDV	I ew100UR	1.84	100	1.80	0.04	R/U

	I ew200UR	1.91	197	1.80	0.003	R/U
	I ew200DR	1.94	200	1.82	0.07	R/D
	I ew200U	1.89	200	1.85	0.010	I/U
	J ew200D	1.94	199	1.88	0.009	I/D
K vwCDV	K vw100UR	1.77	99	1.73	0.013	R/U
	K vw200UR	1.69	200	1.63	0.008	R/U
	K vw300UR	1.65	299	1.57	0.016	R/U
	K vw400U	1.52	400	1.49	0.017	I/U
N ewCDV	N ew350DR	1.53	350	1.52	0.07	R/D
	N ew700D	1.47	698	1.39	0.02	I/D
O ewvwCDV	O ewvw280DR	1.59	280	1.54	0.02	R/D
	O ewvw100D	1.65	100	1.62	0.05	I/D
P wCDV	P w200DR	1.62	200	1.55	0.018	R/D
	P w380UR	1.57	378	1.49	0.02	R/U
	P w170D	1.53	170	1.50	0.018	I/D
	P w800U	1.54	800	1.33	0.038	I/U

R Reconstituted, I Intact, D Drained, U Undrained, p'_c p' at start of shearing, v_0 initial specific volume, v_c specific volume at start of shearing

Table 3: Details of elemental composition for some weathering degrees from EDXS

Weathering degree	Elemental composition (%)																			
	O		Na		Mg		Al		Si		K		Fe		Cl		Ca		Others	
	Wt	At	Wt	At	Wt	At	Wt	At	Wt	At	Wt	At	Wt	At	Wt	At	Wt	At	Wt	At
A ewCDV	41.68	54.46	0.68	0.62	0.78	0.67	7.37	5.71	35.8	26.64	0.3	0.16	5.53	2.07	-	-	-	-	7.86	9.67
B ewCDV	45.51	56.63	0.9	0.78	0.56	0.46	17.33	12.79	23.76	16.84	0.83	0.42	3.85	1.37	-	-	-	-	7.26	10.71
D wmwHDV	43.38	54.8	0.78	0.69	0.42	0.35	11.27	8.44	34.93	25.14	0.45	0.23	2.72	0.98	-	-	-	-	6.06	9.37
E vwwHDV	39.48	48	1.18	1	1.18	0.95	-	-	0.6	0.41	-	-	-	-	0.36	0.2	37.71	18.3	19.5	31.08
J ewCDV	44.18	56.22	-	-	0.75	0.63	14.23	10.74	29.44	21.34	1.58	0.82	4.11	1.5	-	-	-	-	5.72	8.76
P wCDV	43.85	55.41	-	-	0.65	0.54	14.7	11.02	26.95	19.4	2.97	1.53	3.91	1.41	-	-	-	-	6.98	10.69

Wt Weight %, At Atomic %, O Oxygen, Na Sodium, Mg Magnesium, Al Aluminium, Si Silicon, K Potassium, Fe Iron, Cl chlorine, Ca Calcium

Table 4: Details of mineralogy from the XRD

Weathering degree	Minerals (%)			
	Quartz	Feldspars	Clays	Others
A ewCDV	11	-	81	8
B ewCDV	33	33	18	12
D wmwHDV	49	8	11	32
E vwwHDV	34	15	31	20
H wmwCDV	17	18	44	21
J ewCDV	34	24	39	3
K vwCDV	40	18	18	24
P wCDV	34	45	14	7